

MOUNTAIN-PLAINS CONSORTIUM

MPC 16-313 | R. Bridgelall, J.B. Rafert, D.D. Tolliver

Remote Sensing of Multimodal Transportation Systems



A University Transportation Center sponsored by the U.S. Department of Transportation serving the Mountain-Plains Region. Consortium members:

Colorado State University
North Dakota State University
South Dakota State University

University of Colorado Denver
University of Denver
University of Utah

Utah State University
University of Wyoming

Remote Sensing of Multimodal Transportation Systems

Dr. Raj Bridgelall (Co-PI)¹
Dr. James B. Rafert (PI)²
Dr. Denver D. Tolliver¹

¹Upper Great Plains Transportation Institute
²Department of Physics
North Dakota State University
Fargo, North Dakota

September 2016

Disclaimer

The contents of this report reflect the views of the authors, who are responsible for the facts and the accuracy of the information presented. This document is disseminated under the sponsorship of the Department of Transportation, University Transportation Centers Program, in the interest of information exchange. The U.S. Government assumes no liability for the contents or use thereof.

NDSU does not discriminate in its programs and activities on the basis of age, color, gender expression/identity, genetic information, marital status, national origin, participation in lawful off-campus activity, physical or mental disability, pregnancy, public assistance status, race, religion, sex, sexual orientation, spousal relationship to current employee, or veteran status, as applicable. Direct inquiries to Vice Provost for Title IX/ADA Coordinator, Old Main 201, NDSU Main Campus, 701-231-7708, ndsuoaa@ndsu.edu.

ABSTRACT

Hyperspectral remote sensing is an emerging field with many potential applications in the observation, management, and maintenance of the global transportation infrastructure. This report describes the development of an affordable framework to capture hyperspectral images and models to classify the images. The framework and models enable new approaches to plan, analyze, and assess the performance of multimodal transportation systems. Every hyperspectral image frame contains information in wavelengths that extend well beyond those that humans are capable of seeing or perceiving. The rapid size and cost reduction of both unmanned aircraft systems and hyperspectral image sensors enable easy scaling of the framework. Scaling is achieved simply by conducting multiple parallel missions to achieve broad area coverage at affordable prices. The authors showcase the general utility of the framework to enhance models used for roadway congestion forecasting, railway condition monitoring, and pipeline risk management. The authors offer additional insights by demonstrating a specific utility of the framework and models for the rapid detection of hazardous spills. Practitioners who utilize the framework and models to implement hyperspectral remote sensing platforms will benefit from greater situational awareness to make informed decisions in transportation systems development, operations, and maintenance.

TABLE OF CONTENTS

1. Introduction.....	1
2. Part I – Application Barriers and Opportunities.....	4
2.1. Section Introduction	4
2.2. Assessment of Application Barriers	5
2.2.1 Limited Availability of Hyperspectral Remote Sensing Platforms.....	6
2.2.2 Accessibility Limitations of Remote Sensing.....	7
2.2.3 Difficulty of Sensor Miniaturization.....	8
2.2.4 Excessive Latencies in the Image Processing Chain.....	9
2.2.5 Non-Technical Barriers.....	9
2.3. Emerging Opportunities	10
2.3.1 Pushbrooming Framework for Hyperspectral Image Acquisition	10
2.3.2 Hyperspectral Sensor Miniaturization.....	12
2.3.3 Proliferation of Small UAS Platforms	12
2.3.4 Advancements in Computing.....	12
2.4. New Application Utilities.....	13
2.4.1 Utility Enhancement of Existing Applications.....	13
2.4.2 Taxonomy of Hyperspectral Applications in Transportation.....	14
2.4.3 Application Scenario in Highway Asset Management	15
2.5. Section Discussion and Conclusion.....	17
3. Part II – General Framework for Transport Systems Analysis	18
3.1. Section Introduction	18
3.2. General Application of the Framework.....	19
3.3. Scenario Studies and Results.....	20
3.3.1 Roadway Congestion Forecasting.....	20
3.3.2 Railway Condition Monitoring	21
3.3.3 Pipeline Risk Management	22
3.4. Section Conclusion.....	24
4. Part III – Framework Application for Hazardous Spill Detection.....	26
4.1. Section Introduction	26
4.2. Background	27
4.3. Method of Rapid Classification.....	27
4.3.1 Feature Extraction	28

4.3.2 Distance Measure	29
4.4. Results and Discussions	30
4.4.1 Separability Performance	30
4.4.2 Computational Complexity	32
4.4.3 Considerations for Transfer to Practice.....	35
4.5. Section Conclusions	35
5. Conclusions.....	37
6. References.....	38

LIST OF TABLES

Table 2.1	Applications of Hyperspectral Remote Sensing in Transportation	4
Table 2.2	Existing and Planned Spaceborne Hyperspectral Imaging Platforms.	6
Table 2.3	Existing Airborne Hyperspectral Imaging Platforms.	6
Table 3.1	Typical Spatial and Spectral Requirements.....	25
Table 4.1	SSC Separability Matrix for Typical Ground Cover	31
Table 4.2	Class Separability for SAM and SSC.....	32
Table 4.3	Relative Complexities of the Classifiers	35

LIST OF FIGURES

Figure 1.1	Infrastructure Performance Measures Linked to Economic Growth	1
Figure 1.2	Conceptualization of Hyperspectral Remote Sensing.....	2
Figure 2.1	Remote Sensing Tradeoff in Mobility and Accessibility.....	8
Figure 2.2	Optical Configuration of the Hyperion Hyperspectral Remote Sensing Platform.....	9
Figure 2.3	Pushbrooming Approach of Hyperspectral Remote Sensing.....	11
Figure 2.4	Key Sensor Components Targeted for Miniaturization.	12
Figure 2.5	Application Enhancements with High Resolution Imaging.....	14
Figure 2.6	Taxonomy of Hyperspectral Applications in Transportation	15
Figure 3.1	Theoretical Volume-Density Relationship	21
Figure 3.2	The SSC Feature Space for Selected Materials	23
Figure 4.1	Spectral Signatures for Typical Ground Cover.....	29

EXECUTIVE SUMMARY

The global transportation system is massive, open, and dynamic. Existing performance and condition assessments of the complex interacting networks of roadways, bridges, railroads, pipelines, waterways, airways, and intermodal ports are expensive. Hyperspectral remote sensing is an emerging field with potential applications in the observation, management, and maintenance of the global transportation infrastructure. Hence, this research explores the potential for using hyperspectral image analysis to remotely sense and evaluate the multimodal transportation infrastructure.

Unlike panchromatic, color, and infrared imaging, each layer of a hyperspectral image pixel records reflectance intensity from one of dozens or hundreds of relatively narrow wavelength bands that span a broad range of the electromagnetic spectrum. Hence, every pixel of a hyperspectral scene provides a unique spectral signature that offers new opportunities for informed decision-making in transportation systems development, operations, and maintenance.

Few spaceborne systems with hyperspectral image sensors exist. In general, spaceborne systems such as satellites and space stations are capable of capturing images of vast areas in a short period, but they provide lower spatial resolution than airborne systems. Consequently, some practitioners use manned aircraft to achieve higher spatial resolution when needed. However, the additional expense of custom missions and manned aircraft operation reduces the affordability of frequent hyperspectral remote sensing with broad area coverage. Fortunately, the rapid size and cost reduction of unmanned aircraft systems and hyperspectral image sensors promise a third alternative. In addition, such systems are more scalable because practitioners can conduct multiple parallel missions to achieve broad area coverage at affordable prices.

This report summarizes the research in three parts. Part I includes the results of a literature search to assess the application barriers that have traditionally limited the use of hyperspectral remote sensing for transportation applications. The authors formulate an operational framework for a pushbroom type of remote sensing system to achieve both high spatial and spectral resolutions with affordable hyperspectral image sensors. A taxonomy of potential applications subsequently identifies numerous existing and emerging opportunities to apply the framework for transportation systems analysis and performance assessments. Part II explores the utility of the framework in three important and distinct transportation applications: roadway congestion forecasting, railway condition monitoring, and pipeline risk management. A scenario analysis explains the general approach for utilizing hyperspectral image analysis to improve models that practitioners currently use in each of the application areas. Part III showcases detailed use of the framework and models to develop an innovative approach for detecting hazardous spills such as crude oil. In particular, the authors illustrate how using small unmanned aircraft systems with lightweight hyperspectral image sensors would enable resolution agile and real-time remote sensing. This final part includes the development of a new rapid hyperspectral image classification model to enable the real-time remote sensing capability. In summary, practitioners will benefit from using the hyperspectral remote sensing framework to advance the state-of-the-art of transportation systems planning and performance evaluation.

1. INTRODUCTION

The global transportation system is interdependent on the performance of large and complex multimodal and intermodal facilities that move people, goods, and waste. The U.S. transportation infrastructure consists of more than 4 million miles of roadways, 600,000 bridges, 1.5 million miles of above- and below-ground oil and gas pipelines, 100,000 miles of railroad tracks, 25,000 miles of navigable waterways, and 19,000 airports (BTS 2014). Trucks alone carry more than 8 billion tons of goods valued at more than \$10 trillion each year (Bridgelall 2014). All countries rely on a high-performance multimodal transportation infrastructure for sustained economic growth and prosperity. Consequently, the need for regular performance measures of the entire network has become critical.

Climatic factors and heavy vehicle traffic accelerate deterioration. Figure 1.1 illustrates the interdependencies between economic growth and performance measures. Population growth and quality-of-life pursuits drive economic growth, which in turn fuels higher demand to transport more people and goods. To meet those demands while realizing economies of scale, organizations increase the size of the carriers such as trucks, rail cars, ships, pipelines, and aircrafts. Consequently, the infrastructure must bear a higher load density from the aggregate increase in the gross weight of carriers and their miles traveled. Together with climatic factors, an increase in load density accelerates the deterioration rate of surface transportation infrastructure such as roads, bridges, railroads, and runways. Maintaining a state of good repair requires regular performance measures to enable optimized maintenance cycles (Zietsman, et al. 2011). Such practices improve the efficiency and cost-effectiveness of asset management goals to maximize the amount of infrastructure in good condition and to support a sustainable cycle of economic growth.

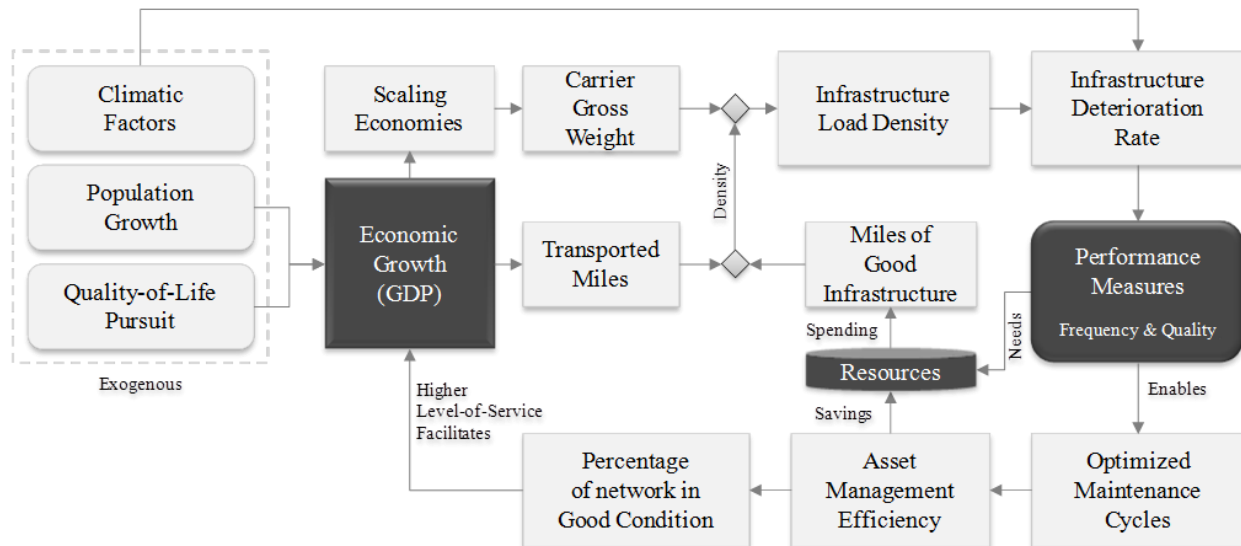


Figure 1.1 Infrastructure Performance Measures Linked to Economic Growth

U.S. highway agencies collectively spend billions of dollars annually to maintain highways (Cambridge Systematics, Inc. 2011). Freight railroads incur similar expense levels (AAR 2014). The old adage that “you cannot fix what you don’t know is broken” highlights the importance of regular performance measurements. Enhanced situational awareness of maintenance needs will optimize resource planning to curb adverse effects of escalating traffic load density. However, existing approaches to network-wide and continuous performance measures are expensive and time-intensive. Most jurisdictions still use manual labor to visually inspect and report on infrastructure condition. In most cases, network capacity diminishes when agencies must close portions of the network to accommodate the operations of non-

destructive evaluation (NDE) and surface scanning equipment (Bridgelall 2013). Hence, agencies everywhere are seeking faster and more affordable ways to collect and analyze data to assess the capacity, performance, safety, and security of the transportation infrastructure. Hyperspectral remote sensing offers an opportunity to meet all of those needs.

Unlike panchromatic, color, and infrared imaging, each layer of a hyperspectral image pixel records reflectance intensity from one of dozens or hundreds of relatively narrow wavelength bands that span a broad range of the electromagnetic spectrum. Hence, every pixel of a hyperspectral scene provides a unique spectral signature that offers new opportunities for informed decision-making in transportation systems development, operations, and maintenance. Figure 1.2 illustrates the concept of a hyperspectral image frame.

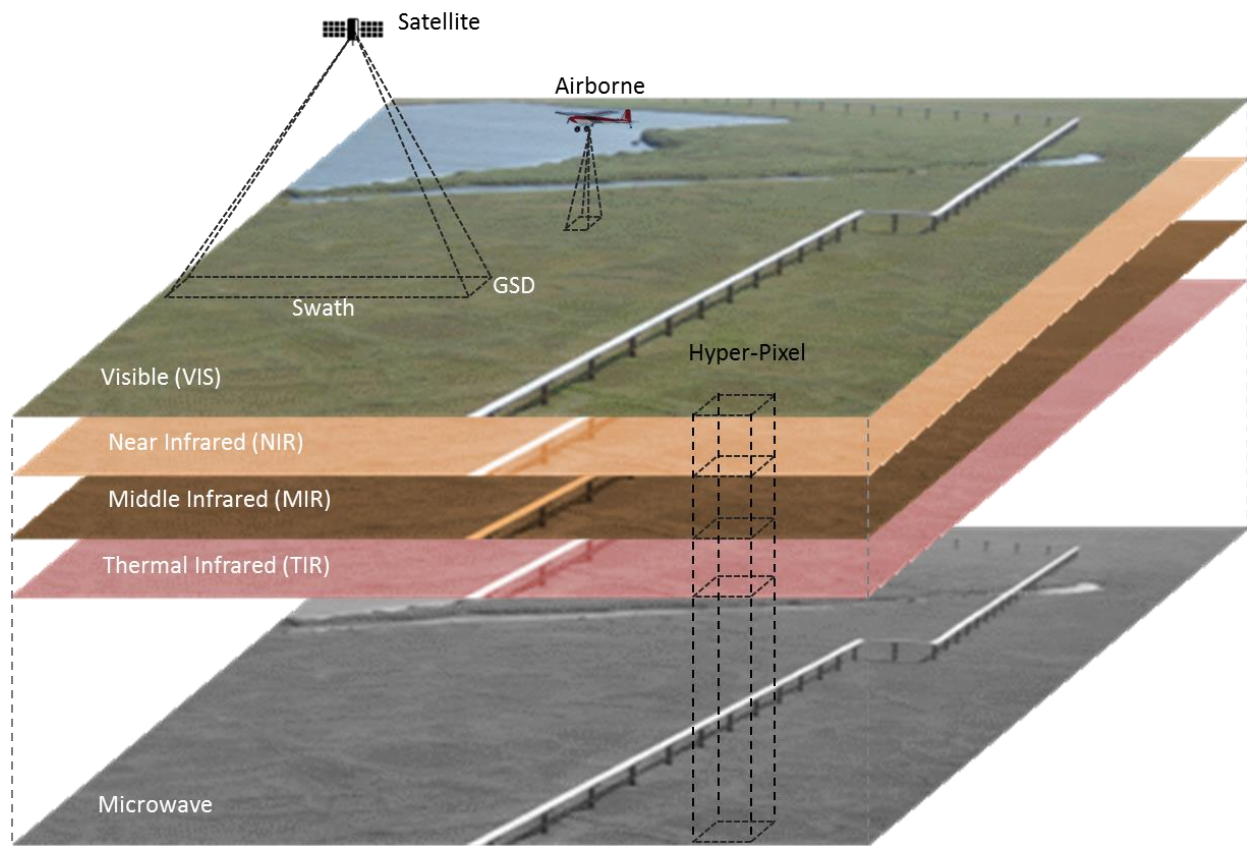


Figure 1.2 Conceptualization of Hyperspectral Remote Sensing

Few spaceborne systems with hyperspectral image sensors exist. In general, spaceborne systems such as satellites and space stations are capable of capturing images of vast areas in a short period, but they provide lower spatial resolution than airborne systems. Consequently, some practitioners use manned aircraft to achieve higher spatial resolution when needed. However, the additional expense of custom missions and manned aircraft operation reduces the affordability of frequent hyperspectral remote sensing with broad area coverage. Fortunately, the rapid size and cost reduction of unmanned aircraft systems and hyperspectral image sensors promise a third alternative. In addition, such systems are more scalable because practitioners can conduct multiple parallel missions to achieve broad area coverage at affordable prices.

Part I of this report includes the results of a literature search to assess the application barriers that have traditionally limited the use of hyperspectral remote sensing for transportation applications. The authors formulate an operational framework and deployment models for a pushbroom type of remote sensing system to achieve both high spatial and spectral resolutions with affordable hyperspectral image sensors. A taxonomy of potential applications subsequently identifies numerous existing and emerging opportunities to apply the framework and model for transportation systems analysis and performance assessments. Part II explores the utility of the framework and models in three important and distinct transportation applications: roadway congestion forecasting, railway condition monitoring, and pipeline risk management. A scenario analysis explains the general approach for utilizing hyperspectral image analysis to improve models that practitioners currently use in each of the application areas. Part III showcases detailed use of the framework to develop an innovative model for detecting hazardous spills such as crude oil. In particular, the authors illustrate how using small unmanned aircraft systems with lightweight hyperspectral image sensors would enable resolution agile and real-time remote sensing. This final part includes the development of a new rapid hyperspectral image classification technique to enable the real-time remote sensing capability.

2. PART I – APPLICATION BARRIERS AND OPPORTUNITIES

2.1 Section Introduction

Remote sensing using spaceborne and airborne imaging platforms offer the key advantage of broad spatial coverage without degrading the infrastructure performance or capacity. Nevertheless, there have been relatively few applications of remote sensing in transportation. Even fewer use techniques involving hyperspectral image acquisition. Table 2.1 summarizes the literature available on remote sensing in transportation at the time of this research. The table indicates which application used a mix of panchromatic (P), color (C), multispectral (M), and hyperspectral (H) types of image acquisition.

It is apparent from the literature review that the year 2000 marked the beginning of transportation-related applications of hyperspectral remote sensing. Government investment in transportation research hastened most of those early activities in the U.S. The Transportation Equity Act (TEA-21) directed the United States Department of Transportation (USDOT) to collaborate with the National Air and Space Administration (NASA) to form the National Consortia for Remote Sensing in Transportation (NCRST). The act resulted in a grant award that initiated the NCRST in 2000.

The objective of this section is to characterize the barriers to hyperspectral remote sensing in transportation, assess the emerging opportunities, and to propose new utilities. The organization of this part of the report is three subsections that 1) assess the requirements from sensors and the data processing, and characterize some of the key non-technical barriers, 2) explore emerging opportunities that address some of the key barriers identified, and 3) introduce transportation application taxonomies that include new ideas to benefit from hyperspectral remote sensing. A scenario study will demonstrate how the models of highway capacity planning could leverage capabilities of remote sensing to update their parameters for improved performance. The final section summarizes and concludes the study.

Table 2.1 Applications of Hyperspectral Remote Sensing in Transportation

Applications	P	C	M	H
Asphalt road surface condition assessment, <i>Institute of Atmospheric Pollution Research & University of Rome, Italy (Mei, et al. 2014)</i>	x	x	x	x
Oil spill detection and impact prediction in ice-affected marine environments, <i>LOOKNorth Center of Excellence for Commercialization and Research, NL Canada (Warren, et al. 2014)</i>		x	x	x
Land use monitoring in response to urbanization, <i>Jawaharlal Nehru University, New Delhi, India (Rani 2014)</i>			x	
Produce road condition indices from panchromatic images available at 46 cm from WorldView-2 (Digital Globe) satellite, the highest spatial resolution available in 2014, <i>University of Colorado at Boulder, CO, USA (Yerasi 2014)</i>	x			
Road condition monitoring from hyperspectral imagery, <i>University of São Paulo, Brazil & the Brazilian Transportation Planning Society, Brazil (Resende, Bernucci and Quintanilha 2014)</i>				x
Three-dimensional image reconstruction of scenes to identify and characterize unpaved road defects, <i>Michigan Tech Research Institute, MI, USA (Dobson, et al. 2014)</i>		x		
Three-dimensional image reconstruction of scenes to identify and characterize unpaved road defects, <i>Geographic Information Science Center of Excellence, South Dakota, USA (Zhang 2013)</i>		x		
Road type classification by distinguishing between asphalt, cement, and unpaved roads and course classification (good, intermediate, bad) of road condition, the <i>University of Applied Sciences, Stuttgart, Germany (Mohammadi, Hahn and Engels 2011)</i>				x

Applications (Continued)	P	C	M	H
Information fusion, including hyperspectral and other remote sensing techniques, for transportation infrastructure surveillance by the Earth Observation and Natural Hazard Technologies Consortium of the <i>European Commission</i> , Italy (Proto, et al. 2010)	x	x	x	x
Use of unmanned aircrafts to monitor construction progress and inventory roadway assets, <i>Utah State University</i> , UT, USA (Jensen, et al. 2009)		x		
Correlate the amount of dead vegetation along pipeline right-of-ways to gas leaks, <i>International Institute for Geo-information Science and Earth Observation & Utrecht University</i> , the Netherlands (Van der Werff, et al. 2008)				x
Pipeline right-of-way monitoring for leak and encroachment detection, <i>Electricore, Inc.</i> , CA, USA (Electricore, Inc. 2007)		x	x	
Trained classification of transportation infrastructure from hyperspectral scenes, <i>Midwest Transportation Consortium, University of Iowa</i> , IA, USA (Sugumaran, Gerjevic and Voss 2007)				x
Automated classification of urban surfaces to distinguish between roofs, roads, and other land features, the <i>German Remote Sensing Data Center</i> , Oberpfaffenhofen, Germany (Heiden et al., 2005) (Heiden, et al. 2007)				x
Pothole identification and road condition assessment, <i>Research Systems Inc.</i> VA, USA, and <i>SpecTIR Corp.</i> , NV, USA (Jengo, et al. 2005)		x		x
Railroad track inventory and use assessment, <i>Humboldt-University, Berlin, Germany & Center for Remote Sensing of Land Surfaces</i> , Bonn, Germany (Damm, Hostert and Schiefer 2005)	x	x	x	
Traffic analysis and forecasting using unmanned aircrafts, University of South Florida, FL, USA (Puri 2005)		x		
Pavement condition assessment, the <i>National Consortia for Remote Sensing in Transportation</i> (NCRST), CA, USA (Herold, et al. 2003)				x
Survey of potential applications of remote sensing, the <i>Aviation Institute at the University of Nebraska and the Nebraska Airborne Remote Sensing Facility</i> , NE, USA (Bowen, Vlasek and Webb 2004)				x
Roadway network extraction from remotely sensed images, <i>Boeing-Autometric Corporation</i> , CO, USA (Penn 2002)				x
Wetland classification for compliance of environmental assessments, <i>North Carolina DOT, EarthData Technologies, Mississippi State University</i> , MS, USA (Mah, et al. 2002)				x
Submerged aquatic vegetation hazard identification for navigable waterways, <i>George Mason University</i> , funded by the EPA and the USGS, VA, USA (Gomez 2002)				x
Classification of features in urban scenes, the <i>University of New South Wales</i> , Australia (Bhaskaran and Datt 2000)				x

2.2 Assessment of Application Barriers

Hyperspectral remote sensing promises significant utility in helping to advance applications in transportation. Although sensors and techniques of hyperspectral remote sensing have existed for several decades, practitioners have deployed only a few applications (Goetz 2009). The subsections that follow will further explore the barriers to adoption that include:

- Limited availability of hyperspectral remote sensing platforms
- Accessibility limitations of remote sensing
- Difficulty of sensor miniaturization
- Extensive latencies in the image processing chain
- Non-technical barriers

These are not necessarily exhaustive but they represent some of the most important barriers.

2.2.1 Limited Availability of Hyperspectral Remote Sensing Platforms

Spaceborne platforms of hyperspectral remote sensing began in the year 2000 with the deployment of the experimental MightySatII.1 (Rafert 2014). As of 2014, only five satellites carry a hyperspectral imaging system. Table 2.2 provides their launch year and summarizes their key sensor operating parameters.

Table 2.2 Existing and Planned Spaceborne Hyperspectral Imaging Platforms.

Satellites	Year	Operator	Type	BL	BU	N	GSD	Swath	Revisit
MightySatII.1	2000	USAF (inactive)	HSI	470	1050	145	30	15	5
EO-1 Hyperion	2000	NASA	HSI	400	2500	220	30	180	16
PROBA-CHRIS	2001	Europe	PAN			1	5	13	7
			HSI	400	1050	19	17	13	
			HSI	400	1050	63	34	13	
HJ-1A	2008	CAST (China)	MSI	430	900	4	30	700	4
			HSI	450	950	115	100	50	
ISS HICO	2009	NASA/ONRL	HSI	380	1000	102	92	42	14
YouthSat	2011	India/Russia	HSI	450	950	63	4000	70	5
HISUI ALOS-3	2015	Japan	HSI	400	2500	185	30	30	60
EnMAP	2017	Germany	HSI	420	2450	222	30	30	4
PRISMA	2017	Italy	HSI	400	2500	200	30	30	7
HyspIRI	2022	NASA/JPL	HSI	400	2500	200	60	145	19

HSI, MSI, and PAN indicate the type of imaging systems as hyperspectral, multispectral, and panchromatic, respectively. BL and BU indicate the lower and upper wavelength bands, respectively. N indicates the number of wavelength channels. The ground sensing distance (GSD) and swath are in meters. The revisit period is in days. Spaceborne services have fixed orbits and they revisit a particular ground area at fixed intervals.

From the literature review, Table 2.3 summarizes some of the most extensively utilized airborne platforms. Operators can schedule flight paths and missions with greater flexibility than spaceborne platforms. However, their operation may require special permits and approvals to enter restricted airspace above the targeted ground area. Secondly, airborne missions are limited to a shorter window of the day when the sun angle is within the desired range for proper illumination, whereas satellites maintain a sun synchronous orbit to achieve constant illumination.

Table 2.3 Existing Airborne Hyperspectral Imaging Platforms.

Airborne	Owner	BU	BL	IFOV	N	FOV	F_r	Max Speed
AVIRIS	NASA/JPL	360	2500	1.0	224	677	100	730 km/h
HyMap	HyVista Corporation	450	2500	2.5	128	512	500	837 km/h
ProSpecTIR	SpecTIR	400	2500	1.3	244	320	100	210 km/h
CASI 1500H	Itres Research, Canada	380	1050	0.49	288	1500	85	223 km/h
HySpex	Norsk Elektro Optikk	400	2500	0.75	256	1600	100	263 km/h
APEX	European Space Agency	380	2500	0.48	508	1024	43.4	310 km/h

Table 2.3 includes the instantaneous field-of-view (IFOV) per pixel of the optical system in milliradians (mr) and the total detector field-of-view (FOV) in number of spatial pixels. For comparison with the spaceborne platforms, the GSD $\Delta\phi_x$ varies with flight altitude h_s as

$$\Delta\phi_x = 2h_s \tan\left(\frac{IFOV}{2}\right). \quad (1)$$

For small angles, $\tan(\theta) \approx \theta$, hence $\Delta\phi_x \approx h_s \times \text{IFOV}$. The frame rate F_r of the optical system is in frames per second and the maximum speed of the aircraft is in km/h.

2.2.2 Accessibility Limitations of Remote Sensing

Remote sensing is a type of non-destructive evaluation (NDE) method that complements surface scanning techniques. Hyperspectral systems provide signature recognition capability for many targets that other methods, such as multispectral and infrared remote sensing, cannot discriminate.

The technique relies on how light of different wavelengths interact with the unique composition and the variations in particle sizes at the molecular level. The diffraction, refraction, and reflection of incident light are unique at the different narrow band wavelength regions. Remotely sensed imagery from satellites provides a birds-eye view of the ground; therefore, shadowing from trees and other large objects will occlude visibility. Although satellites can revisit areas in several days, cloud cover could hamper image acquisition. The atmosphere absorbs transmitted and reflected irradiance. This loss in energy reduces signal intensity and adds background noise. In addition, dust, dirt, or moisture on surfaces can reduce the image quality.

The use of a mix of remote sensing platforms involves a tradeoff between mobility and accessibility as illustrated in Figure 2.1. Airborne sources provide significantly less area coverage because of their lower mobility. However, they do offer greater degrees of accessibility that addresses some of the visibility issues of spaceborne sources. Manned aircrafts still have limited accessibility to provide the resolution needed to monitor some aspects of the transportation infrastructure. For example, transverse pavement cracks become visible with one-meter resolution and manhole covers become visible at the centimeter resolution scale (Bowen, Vlasek and Webb 2004). Unmanned aircraft systems (UASs) promise even higher accessibility and resolution, but their substantial reduction in mobility increases the time needed per unit to monitor a vast transportation network. A fleet of UASs could remediate the mobility shortcoming but at the expense of additional training, maintenance, and operating costs. Even with higher resolution remote sensing, it remains infeasible to measure some physical parameters such as ride quality, which is an important indicator of road condition (Bridgelall 2014).

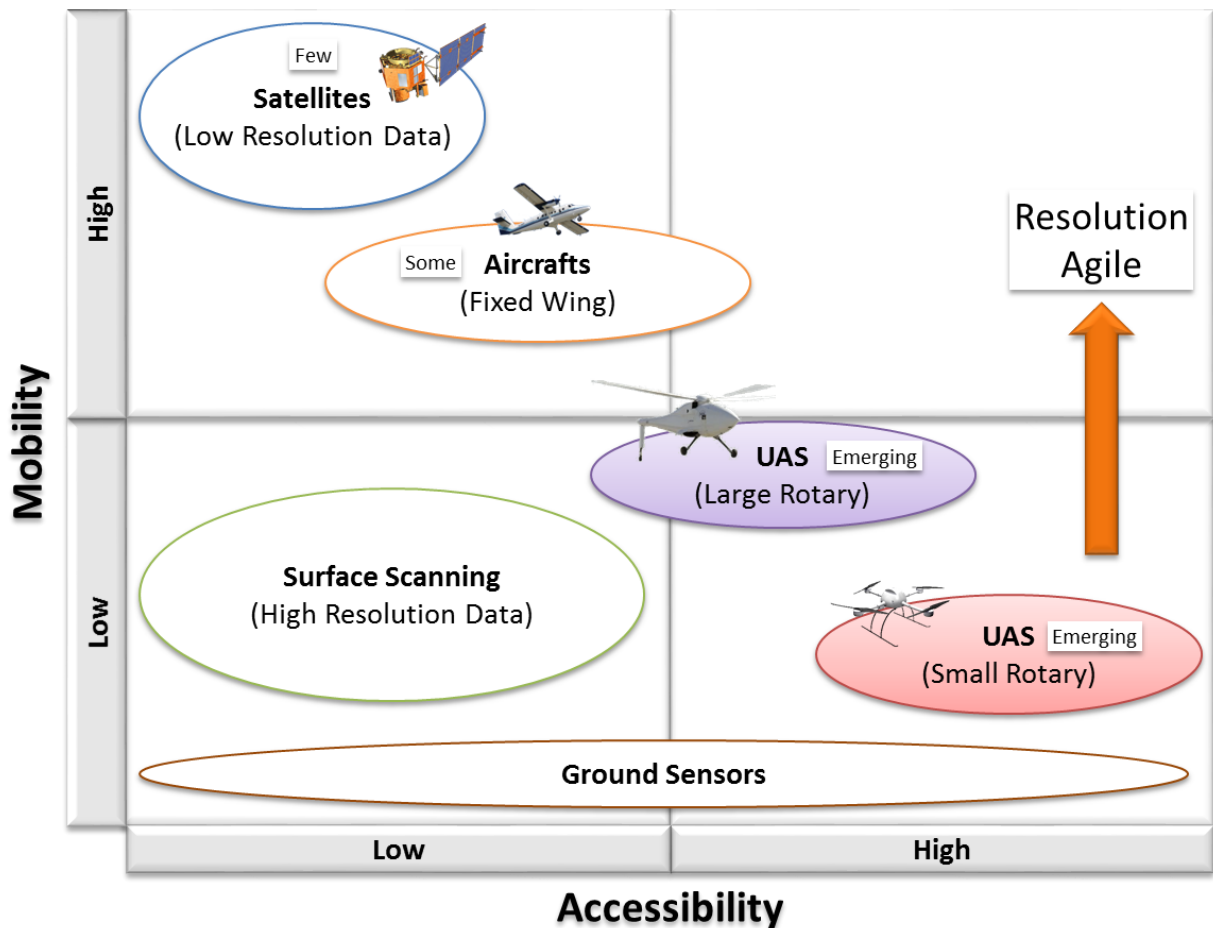


Figure 2.1 Remote Sensing Tradeoff in Mobility and Accessibility

2.2.3 Difficulty of Sensor Miniaturization

Techniques of wavelength separation involve high quality prisms, diffraction grating, or interferometers. Prisms use the principle of refraction that separate EM wavelengths based on their speed differences through transparent but denser than air media. Gratings use the principles of diffraction and interference; their mass production relies on an ability to create nanometer-scale temperature-stabilized grooves. Interferometers use the principle of constructive interference from EM phase alignment. Their construction relies on the ability to machine temperature-stabilized and nanometer-scale precision optical blocks with integrated beam splitters. These stringent precision requirements establish the need for minimum size and dimension requirements to maintain material strength and operating stability across a large temperature range. The focusing elements are lenses, curved mirrors, or combinations of those. Their design requirements, such as long focal distance, shock resistance, and temperature stability, set stringent design constraints that prevent scaling their construction below certain minimum dimensions.

Figure 2.2 shows the optical configuration of the Hyperion imager that NASA deployed on the EO-1 satellite (Pearlman, et al. 2001). The unit weighs 49 kg (~ 108 lbs.) and has a volume of approximately 0.2 cubic-meters, which is about 25 times the volume of a regulation size basketball.

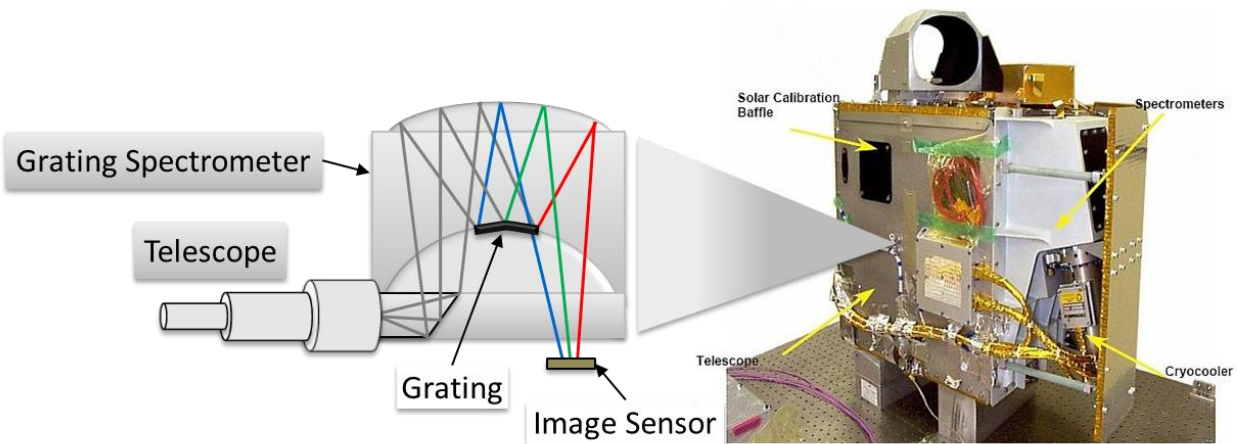


Figure 2.2 Optical Configuration of the Hyperion Hyperspectral Remote Sensing Platform

2.2.4 Excessive Latencies in the Image Processing Chain

Existing spaceborne and airborne services to acquire hyperspectral images require an application process that can take weeks or months and then a subsequent scheduling of the mission (Barry 2001). Once initiated, the flow of data from the image capture platform to the user is relatively slow. The EO-1 satellite revisits the same ground area every 16 days, but weather and cloud cover can prevent image acquisition. Once cleared, the satellite requires 10.5 minutes of lead time before collecting the scene, and about 4 minutes of additional time to collect calibration data. The typical scene collection time is 30 seconds. After downlink, the ground station forwards the raw data to NASA for ‘Level 0’ processing to decode, parse, validate, aggregate, and format the data. NASA can take up to five days to complete the Level 0 processing. Subsequently, NASA sends the data on tape via surface mail to TRW Inc. for ‘Level 1’ processing to apply radiometric calibration and data interpolation. TRW then returns the processed data to NASA within three days for distribution. The user then performs image classification using a variety of supervised and unsupervised methods that are relatively computational complex. The process for existing airborne platforms is similarly extensive. For instance, the USGS suggests that researchers must allocate one to four months after AVIRIS data collection before receiving the processed image files.

2.2.5 Non-Technical Barriers

In addition to the technical and process impedances presented in the previous sections, there are numerous non-technical barriers. They include regulatory restrictions on flight missions, privacy concerns, liability, and the lack of standards.

FAA Restrictions

The Federal Aviation Administration (FAA) banned commercial UAS operations until the agency can address its safe operations among non-cooperative aircrafts and other airborne operations (Abid, et al. 2014). As of 2014, the FAA requires certificates of authorizations (COAs) to conduct research at one of the six national test sites.

Privacy Concerns

The public is generally concerned about the loss of privacy from the practice of capturing images remotely, particularly when using small UASs with integrated cameras. The national press regularly

highlights cases that involve the use of drones by law enforcement agencies to conduct investigations. Such reports tend to awaken concerns about the legality of such surveillance and the potential violation of civil liberties (Abid, et al. 2014).

Liability

As image acquisition devices reduce in size, researchers will likely install them on small UASs. The severity of a UAS failure depends on the type, size, and propulsion option of the UAS. Fuels can ignite in the event of a crash (Abid, et al. 2014). Some UAS crashes have involved injury and property damage. Pilot distraction, similar to the notion of distracted driving, is another area of concern.

Lack of Standards

Contemporary systems for hyperspectral data acquisition consist of a broad range of sensors, platforms, resolutions, and image quality. The transportation industry currently lacks standards for image treatment within and across different acquisition platforms, spectral libraries, timeframes, and meteorological conditions. There are no standard recommendations for the systematic removal of sensor bias, geometric distortions, and radiometric non-uniformity. In addition, relatively few efforts incorporate atmospheric correction. Assembling full scenes from a mosaic of smaller swaths can introduce significant geometric and alignment errors. A first step in addressing the challenges posed by this situation is the systematic acquisition of spectral libraries using standard procedures, sensor settings, illumination, and meteorological conditions.

2.3 Emerging Opportunities

This section reviews the pushbrooming approach to hyperspectral image sensing and illustrates how the technique leverages sensor size reduction to enable use on small UAS platforms and small satellites. Advancements in computing that include more computationally capable microprocessors and cloud-computing techniques are also enablers of the pushbrooming approach when deployed on small UASs.

2.3.1 Pushbrooming Framework for Hyperspectral Image Acquisition

The typical image sensor is a planar two-dimensional (2D) array of $x \times y$ photosites. The sensor has one electronic photosensor beneath each photosite to produce one pixel of the digital image. Most single chip color imagers include a color filter array, such as a Bayer filter mosaic, to pass energy from red (R), green (G), and blue (B) wavelength bands onto the individual photosensors of each photosite. To render the image, de-mosaicing image processing algorithms must subsequently interpolate light intensity from neighboring pixels to produce intensity values for the other two wavelength bands such that the final color image data will map one R-G-B triplet to each pixel of the image sensor. Other approaches use beam splitters or wavelength selective optical filters with multiple sensor arrays (Gilder 2005). A hyperspectral scene is a meta-data cube where each layer is a picture of the same scene sensed at a different wavelength band of the electromagnetic (EM) spectrum. Hence, the color imaging approaches do not scale much beyond the three R-G-B wavelength bands to accommodate the hundreds of wavelength bands of hyperspectral scenes.

A pushbrooming framework for image acquisition enables the use of standard 2D photosensor arrays with pixel size $c_x \times c_y$. This technique sweeps a narrow field-of-view (FOV) of dimensions $(N_x \times \Delta\phi_x) \times \Delta\theta_y$ along the ground path of the flight trajectory. The aperture of a pushbrooming imaging system limits the FOV to one row of the image sensor that contains N_x pixels as illustrated in Figure 2.3. The optical magnification factor for square pixels is $M_\eta = (c_x/\Delta\phi_x)^2$. Wavelength separating optics focus the EM energy from different wavelength bands onto each row of the image sensor. Therefore, each captured

frame of the 2D image sensor will contain the equivalent of one row of the image, but each row will register the same image from a different wavelength band. Hence, a relatively constant speed V_G will improve the quality of the hyperspectral scene assembled from the sequence of image frames.

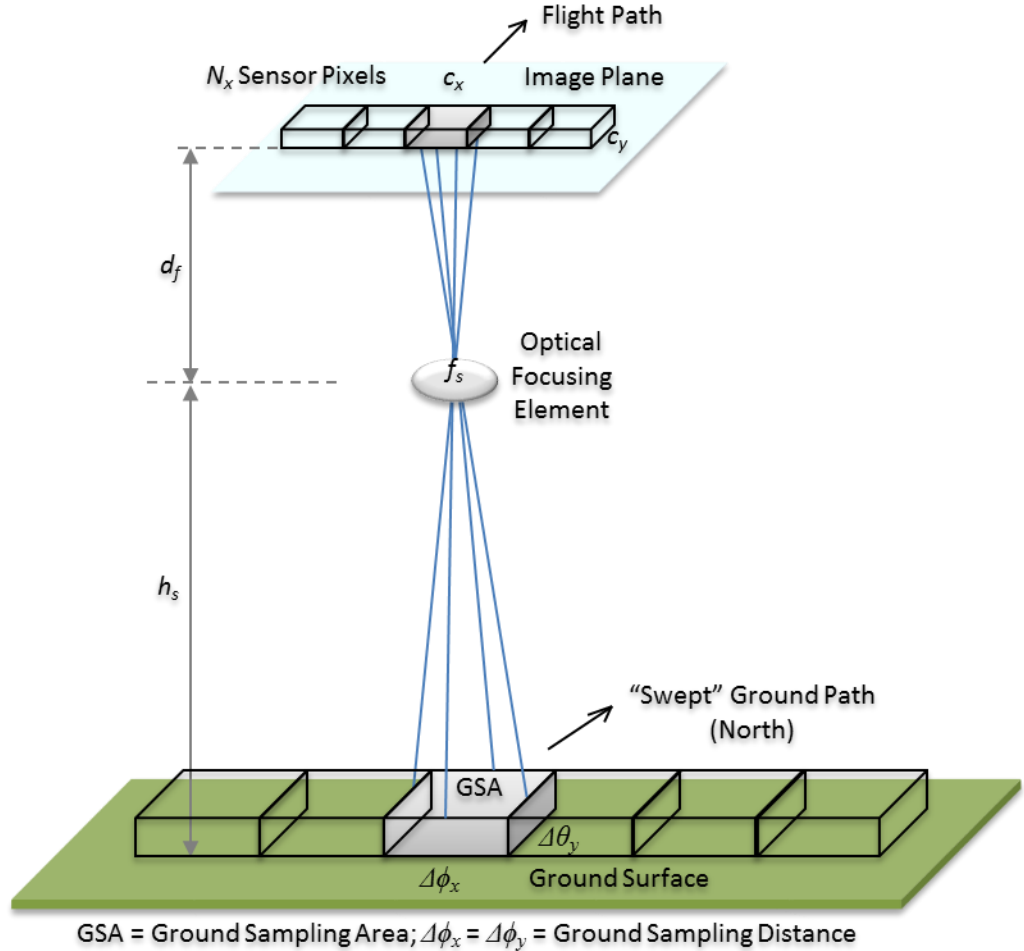


Figure 2.3 Pushbrooming Approach of Hyperspectral Remote Sensing

Some amount of FOV overlap γ will be necessary to aid the image assembly algorithm. Altogether, the constraints of the pushbrooming geometry dictate a minimum image capture frame rate F_m of

$$F_m = \frac{V_G}{c_y \sqrt{M_\eta} (1 - \gamma)}. \quad (2)$$

The Hyperion imager aboard the EO-1 satellite uses this approach and likely requires less FOV overlap than an airborne platform because of its relatively constant speed above the atmosphere. Airborne platforms will dictate an FOV overlap requirement that depends on the expected ride quality at the selected flight altitude and speed. The relative instability of small UAS platforms will also dictate more computationally complex approaches for image frame assembly, image noise reduction, geometric correction, and image classification.

2.3.2 Hyperspectral Sensor Miniaturization

Although the miniaturization of the focusing and wavelength separation elements continues to pose significant challenges, there has been some progress. Figure 2.4 illustrates the key components of a hyperspectral camera. Advancements in precision machining enable the mass production of transmissive holographic diffraction gratings that implement the wavelength separation method (Muslimov 2014). The ability to create microlenses and to integrate aberration-corrected optical elements directly on top of the image sensor enables significant size and cost reduction of the light focusing element (Lambrechts, Tack and Pessolano 2011).

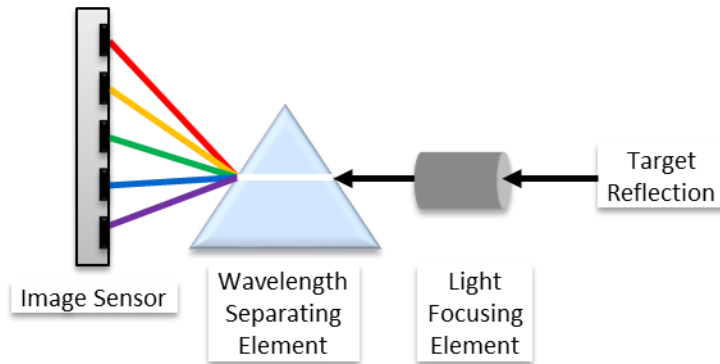


Figure 2.4 Key Sensor Components Targeted for Miniaturization

The ubiquitous adoption of image sensors for mobile phones results in the continuous quest for their performance enhancement and cost reduction. Several manufacturers currently leverage these trends to produce hyperspectral imagers that weigh less than 2 kg (less than 5 lbs.) and those are suitable for installation on small UAS platforms (Colomina and Molina 2014).

2.3.3 Proliferation of Small UAS Platforms

Lower building costs and a proliferation of commercial applications for UASs has led to their widespread use (Abid, et al. 2014). In 2014, the FAA issued exemptions to the commercial movie and television production industry that allow small UAS operations but with various restrictions (FAA 2014). At the time of this report, the FAA issued new operational rules governing routine commercial use of small UASs that clarified many of the previous restrictions (Federal Aviation Administration 2016). These evolving FAA regulations to integrate UASs fully into the airspace will likely continue to spur growth for smaller and more affordable aircrafts. Large organizations such as Amazon, Google, and Facebook announced their intent to deploy small UASs for a variety of commercial purposes. Analysts expect that the UAS industry will spend \$89 billion by 2023 to develop more useful, safer, and easier-to-fly aircraft (Berger 2014). These trends will continue to challenge sensor manufacturers in the size, power, and weight reduction of hyperspectral imaging systems.

2.3.4 Advancements in Computing

The collection, processing, and interpretation of hyperspectral data involve significant computing resources. Image processing involves radiometric calibration, atmospheric correction, geometric alignment, and image stitching. Radiometric calibration involves the removal of temporal or spatial brightness variations in images that are associated with the image sensing system rather than the actual scene reflectance. Through wavelength selective absorption, scattering, and diffraction, the atmosphere modifies the target irradiance both spatially and spectrally, and those modifications change with time. The

amount of unwanted light depends on the atmospheric conditions at the time, the terrain of the scene, and the flight altitude. Atmospheric correction algorithms attempt to estimate and compensate for atmospherically induced variations in irradiance. Off-nadir viewing from pushbroom operations distorts three-dimensional (3D) image projections onto two-dimensional (2D) planes (Clark, Livo and Kokaly 1998). Geometric correction entails knowing the instantaneous position and attitude (orientation) of the platform at the time of image acquisition.

Image classification is a significant aspect of the interpretation and decision-making process. The classification methods and algorithms vary widely but they generally fall into two categories: supervised or unsupervised (Mather and Tso 2003). Supervised methods involve both statistical and machine learning approaches. The computation generally requires a complex calculation between every hyper-pixel and the end member of a spectral class (Gao, et al. 2013). The algorithms of unsupervised methods are generally at least $O(PN^2+N^3)$ computationally complex (Du and Fowler 2008). P is the number of pixels, and N is the number of bands. The continuous advancement and proliferation of multi-core processors, digital signal processors (DSP), and cloud computing architectures could now accommodate these complexities with greater ease.

2.4 New Application Utilities

This section illustrates how a pushbroom framework and associated model of hyperspectral remote sensing could enhance the utility of existing transportation applications as well as create new utilities. To focus the illustration, this section selects road condition assessments for the scenario study. The taxonomies of transportation applications introduced reveal numerous applications that could benefit from hyperspectral remote sensing. The scenario analysis selects highway capacity planning to demonstrate the link between theory and practice using results of the hyperspectral image classification.

2.4.1 Utility Enhancement of Existing Applications

More than 94% of the 4 million miles of paved roads in the United States contains asphalt. The material also covers about 85% of the nation's airport runways and parking areas (NAPA; EAPA 2009). Hyperspectral remote sensing offers numerous utilities in the assessment of roadway surface conditions. Asphalt is easily discernible from other road types because the hydrocarbon of the bitumen binder has maximum absorption bands between 1730 nm and 2300 nm (Cloutis 1989). New asphalt has generally low reflectance (albedo) because bitumen absorbs solar radiation throughout the 250 – 2500 nm range (Heiden, et al. 2007). Deeper absorption bands also indicate newer roads (Smejkalová and Bujok 2012). The average reflectance across the EM spectrum increases as a pavement loses its bitumen surface from erosion and tire polishing (Herold, et al. 2008). With the loss of binder material, aggregate outcropping begins to reveal its mineral signatures (Mei, et al. 2014). Severe pavement cracking could decrease albedo by about 7% because of shadowing and scattering effects (Herold, et al. 2003). Hence, agencies could use hyperspectral remote sensing to catalog the age and relative condition of pavements.

Improved condition assessment accuracy is also possible by analyzing higher resolution images from UAS platforms. As cracks develop, higher resolution images reveal a sharpening of the hydrocarbon features from the exposed layers of the original asphalt mix beneath. Water inlets create absorption bands in the longer wavelength regions. As water interacts with material beneath, iron absorption peaks also appear at 520, 670, and 870 nm (Meer, et al. 2012).

The age and surface condition of pavements are important asset management parameters but agencies are generally more concerned about characterizing their ride quality. Although there is generally a strong correlation between the age of a road and the ride quality it provides, the former is not necessarily an indicator of the latter. For instance, agencies often characterize the ride quality of new roads to assess the

contractor’s performance and to determine fee penalties based on overall roughness. Hence, estimating the age of the pavement from its albedo and the sharpness of its hydrocarbon spectral features alone is not necessarily sufficient information to characterize its ride quality, which is a task that nearly all state highway agencies undertake annually (Bridgelall 2014).

The higher resolution and greater accessibility of UASs could yield 3D images that also enable texture analysis.¹² The combined information obtained from a pushbrooming approach using UAS platforms could result in an ability to classify ride quality qualitatively as shown in Figure 2.5.

Ride Quality	Poor	Albedo (Low) Hydrocarbons (Strong) Texture (Ruts)	Albedo (High) Hydrocarbons (Weak) Texture (Cracks, Potholes, Ruts)
	Good	Albedo (Low) Hydrocarbons (Strong) Texture (Smooth)	Albedo (High) Hydrocarbons (Weak) Texture (Smooth)
		Young	Old
Asphalt Pavement Age			

Figure 2.5 Application Enhancements with High Resolution Imaging

2.4.2 Taxonomy of Hyperspectral Applications in Transportation

The transportation applications that can benefit from utilizing hyperspectral remote sensing fall into the following two groups: a) planning and development and b) maintenance and operations. Figure 2.6 illustrates the taxonomy. The first group has two sub-categories, namely capacity planning and environmental assessment. Likewise, the second group has two sub-categories, namely infrastructure monitoring, and safety & security. Sustainable transportation development means that actions taken today must not adversely affect the ability of future generations to thrive. Hence, planning in transportation focuses on how to design and manage the system capacity and assets to accommodate the mobility and accessibility demands of travel, now and in the future. Developments must be sustainable as population, traffic, and production grows. Therefore, planners aim to minimize adverse impacts to the environment while accommodating the demands. Infrastructure monitoring involves multimodal performance measures as previously described. Safety and security aspects of transportation involve a variety of risk management and emergency response measures as the taxonomy indicates. Future research will expand on the details of how hyperspectral remote sensing provides utility and benefits for each of these areas. As an example, the next section provides a scenario study for one specific area.

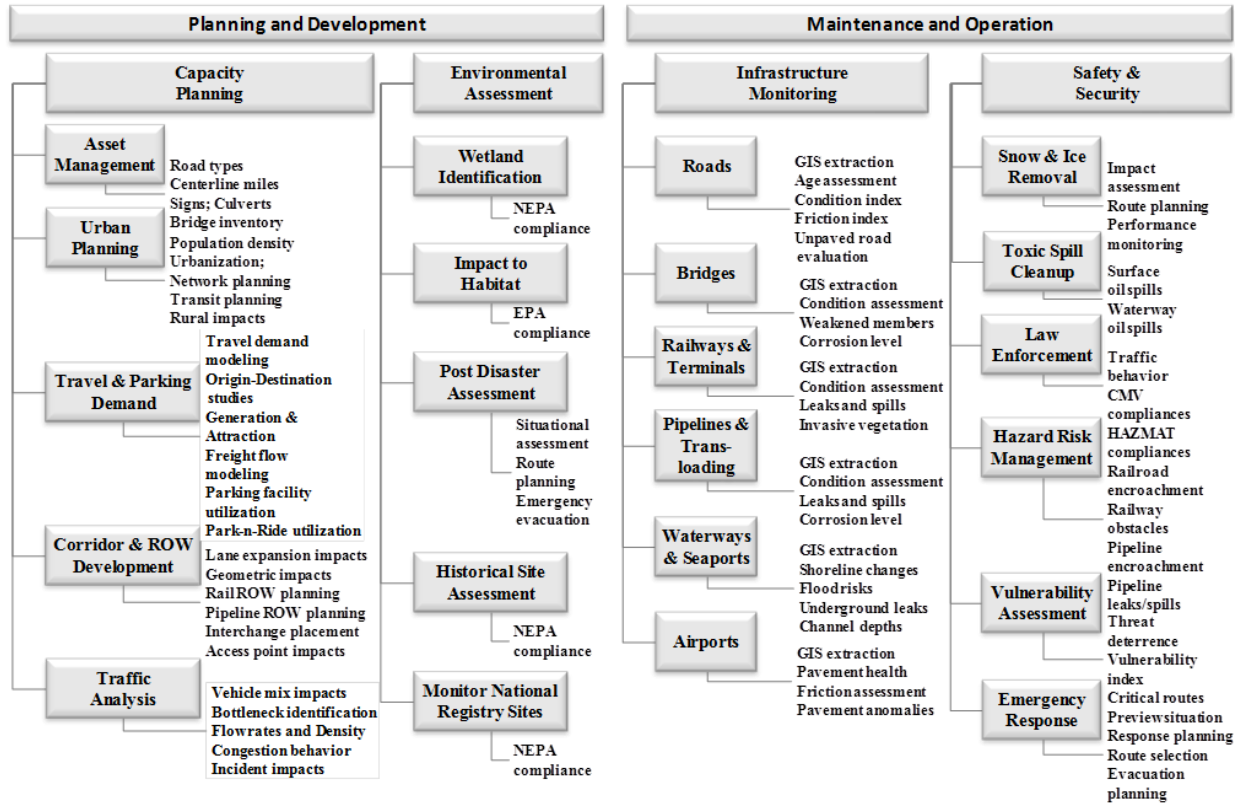


Figure 2.6 Taxonomy of Hyperspectral Applications in Transportation

2.4.3 Application Scenario in Highway Asset Management

The capacity of a transportation network depends on the density and speed at which traffic can safely flow through its corridors. To illustrate how data from hyperspectral remote sensing could be valuable in planning, this section first develops the capacity and operational models for freeways.

The models then provide insights for practitioners to incorporate remotely sensed data to update their various parameters for improved accuracy in analyzing different portions of the complex network. Roadway capacity depends on numerous factors that include functional class, geometry, terrain, traffic mix, peak hour volume, and driver familiarity with the route. The Highway Capacity Manual (HCM) of the Transportation Research Board (TRB) is the accepted standard for highway capacity and level of service determination (HCM 2000).

Freeways are divided highway facilities with full control of access because regulations limit their access to certain types of vehicles, and their access points are limited to specific locations. They typically have two or more lanes for the exclusive use of through traffic in each direction, and the HCM defines their capacity C_f as

$$C_f = 1700 + 10 \times S_{ff} \quad (3)$$

where S_{ff} is the free-flow speed. The base free-flow speed S_{bff} is a function of the speed limit, whereas the free-flow speed is the speed at which drivers feel comfortable traveling the facility. Hence, adjustments to the base free-flow speed produce the free-flow speed as follows:

$$S_{ff} = S_{bff} - f_{LW} - f_{LC} - f_N - f_{ID} \quad (4)$$

where f_{LW} , f_{LC} , f_N , and f_{ID} are adjustment factors that account for non-ideal lane widths, lateral clearance, number of lanes, and interchange density, respectively. To calculate the level-of-service provided, the HCM converts the peak hour volume of vehicles V_T to passenger car equivalents (PCE) or V_{PCE} where

$$V_{PCE} = \frac{V_T}{f_{PH} \times N_L \times f_{HV} \times f_p} \quad (5)$$

in units of passenger cars per hour per lane (pcphpl). The number of lanes in one direction is N_L and the factor that accounts for driver familiarity with the facility is f_p . The default driver-population factors for urban and rural highways are 1.0 and 0.975, respectively. The peak-hour factor f_{PH} is an indicator of the cyclical variations in traffic distribution through the segment for any given day. It is the ratio of the *vehicle* volume in the peak hour period V_{60} to the vehicle volume in the peak 15-minute period V_{15} of that hour such that

$$f_{PH} = \frac{V_{60}}{4 \times V_{15}}. \quad (6)$$

The default peak-hour factors for urban and rural areas are 0.92 and 0.88, respectively. Heavy vehicles require more time-headway than passenger cars to accommodate their limited acceleration and maneuverability on different terrain. Hence, a heavy vehicle factor f_{HV} will normalize the traffic mix to passenger car equivalents. The f_{HV} factor is

$$f_{HV} = \frac{1}{1 + P_T(E_T - 1) + P_R(E_R - 1)} \quad (7)$$

where P_T and P_R are the proportions of trucks (and busses) and recreational vehicles, respectively. E_T and E_R are corresponding terrain-dependent model parameters provided in tables of the HCM. The ability to identify and classify vehicle types as well as traffic density using hyperspectral remote sensing provides a low-cost means to update the model parameters regularly, or for individual jurisdictions.

A popular model for the non-linear change in average speed S_{av} with volume is (Roess, Prassas and McShane 2011):

$$S_{av} = \frac{D_s}{T_{AADT}} \left[1 + \gamma_s \left(\frac{V_{PCE}}{C_s} \right)^\rho \right] \quad (8)$$

where T_{AADT} is the annual average daily travel time for vehicles traveling a segment of length D_s and capacity C_s . Using hyperspectral remote sensing to update the average speed, travel time, and volume of a segment will update the model parameters γ_s and ρ . The average speed S_{av} relates to the traffic density D_{PCE} as follows:

$$D_{PCE} = \frac{V_{PCE}}{S_{av}} \quad (9)$$

in units of passenger cars per mile per lane (pcpmpl). Remotely sensed data can regularly identify the average speed and density of vehicles across any segment of the roadway. The high spectral contrast between manufactured and natural surfaces improves the classification accuracy to determine geometric factors such as lane widths, number of lanes, shoulder clearances, median type, terrain type, and access point or interchange densities, even from relatively low-resolution satellite images. The current version of the highway capacity model does not include a factor that accounts for the influence of surface condition on average speed. Hence, the ability to estimate a condition index using the method described in Figure and calibrating for the average speed and density observed for different facilities will further improve the model. The emerging opportunities that would enable real-time hyperspectral remote sensing also introduce the possibility of adaptive modeling. Such capabilities would enable the adaptive models to account for short-term changes in traffic conditions, incidents, and weather events that affect corridor capacity. This general approach is applicable to multimodal capacity estimation that includes railways, pipelines, and waterways.

2.5 Section Discussion and Conclusion

The increasing loads from heavy vehicles that support growth in commerce accelerate infrastructure deterioration. Agencies adopt asset preservation practices to prolong the service life of infrastructure. However, they lack the resources needed to monitor asset condition with the frequency necessary to identify their optimized maintenance cycles. The multimodal transportation infrastructure is vast and dynamic. Existing methods of condition and performance assessments are laborious and expensive. This research highlighted the emerging opportunities for hyperspectral remote sensing to address the resource gaps and to provide broad coverage and timely assessments. The barriers to deployment identified provided some insights to explain the lack of hyperspectral remote sensing utility in transportation applications. The analysis highlighted five barriers to deployment. Among them, the accessibility limitations of existing sensor platforms and their extensive process chain latencies burden transportation applications that require high-resolution images and rapid results. The other three barriers that include a lack of imaging platforms, bulky sensors, and regulatory constraints are common to most other applications such as precision agriculture. However, emerging opportunities that are countering those barriers include the popularization of UAS utility in consumer applications, sensor miniaturization, and advancements in computing. In particular, the pushbrooming method of hyperspectral image acquisition leverages the cost and size reduction trends of conventional image sensor systems that are now common in nearly all mobile phones. These emerging opportunities also enhance the benefits of applying hyperspectral remote sensing to existing applications in transportation such as pavement condition assessment. These opportunities create new utilities in nearly all categories of transportation applications. This research used the scenario of highway capacity planning to demonstrate a link between the models and the practice of updating them by extracting relevant data from the analysis of hyperspectral scenes. Future opportunities that enable real-time hyperspectral remote sensing will lead to adaptive multimodal models that account for short-term changes that affect corridor capacity.

3. PART II – GENERAL FRAMEWORK FOR TRANSPORT SYSTEMS ANALYSIS

This section illustrates opportunities to utilize the hyperspectral remote sensing framework to develop improved models for a few select applications in transportation. The section presents a generalized approach for applying the framework to develop the models and then offers three specific application scenarios to demonstrate their utility. The selected scenarios explain the models used to analyze roadway mobility, railroad energy consumption, and pipeline risk management. The core concept is to identify specific applications that can benefit uniquely from both the high spatial and high spectral resolutions of hyperspectral remote sensing.

3.1 Section Introduction

While hyperspectral remote sensing has rapidly emerged as a mature field since the early 2000s (Rafert 2014), relatively few applications of hyperspectral analysis in transportation currently exist. As of January 2015, there were only 14 applications reported in the worldwide literature (Bridgelall, Rafert and Tolliver 2015). Early research concluded that the high uncertainty and latency of results from existing airborne and spaceborne platforms create major impediments to the widespread use of remote sensing for applications in transportation (Brecher, Noronha and Herold 2003). Nevertheless, the growing popularity and capabilities of small, low-cost unmanned aircraft systems (UASs) coupled with the steady advancement of lightweight hyperspectral imager payloads of decreasing cost promises vast improvements in mobility, accessibility, spatial resolution, and image quality. However, the government regulations and privacy concerns of many countries continue to hinder the deployment of UASs for commercial applications (TRB 2003). Even at the conclusion of rulemaking and policy enactment, the global transportation industry will need to promote awareness of hyperspectral remote sensing as a viable alternative to terrestrial methods. Agencies will need to train a workforce with the new skills needed to capitalize on these emerging opportunities in remote sensing in general and hyperspectral analysis in particular. As corporations and nations launch low-cost hyperspectral imaging satellites, and small UASs equipped with hyperspectral image sensors proliferate, new applications in the transportation sector are likely to emerge rapidly.

The global transportation network is expansive, dynamic, multimodal, interdependent, and accommodates a diverse range of human behaviors and needs. Analysts study such complex networks by using models to characterize, understand, and predict their behavior, economics, and risks. The accuracy and utility of those models depend on the quality and frequency of data available to quantify their operational parameters and validate their explanatory variables. Beyond improved modeling capabilities, hyperspectral remote sensing and joint spatial-spectral analysis offers the potential to provide regular and accurate information to enable adaptive transportation infrastructures that would support the future operation, safety, and security of connected and autonomous vehicles.

The organization of the remainder of this section is as follows: Section 3.2 introduces the general framework to link transportation systems analysis and hyperspectral analysis. The authors then introduce a range of applications where they foresee high utility for hyperspectral analysis within the general framework. Section 3.2 presents specific scenario analysis covering three different application areas to demonstrate how the outputs of hyperspectral image classification would improve models that practitioners use currently to study a variety of transportation networks. Section 3.4 discusses the results and concludes this section of the report.

3.2 General Application of the Framework

Practitioners worldwide are seeking cost-effective and simplified tools to help them address numerous problems that arise continuously from the massive, open, dynamic, and multimodal global transportation network. According to data from the Central Intelligence Agency, approximately 40 million miles of roadways, 1.4 million miles of navigable waterways, and more than 40,000 airports cover the planet's surface. This infrastructure also includes an interacting and interdependent network of railways, pipelines, and shipping ports along with their associated geological and oceanographic structures.

The most serious problems include reducing congestion, energy consumption, polluting emissions, crash risks, and managing the safety and security of hazardous transport. The growing worldwide population and international commerce drives increasing demands for mobility and accessibility across the global network. Hence, solutions must have the capacity to scale internationally, the ability to provide results in real time, and the propensity for standardization. Hyperspectral remote sensing with fleets of ground-based or UASs offers such an opportunity. Combinations of spatial and spectral data are central to the hyperspectral analysis of scenes from many elements of the global transportation infrastructure. Practitioners with the appropriate training in hyperspectral remote sensing will gain the ability to capitalize on their capabilities and capacity to solve complex transportation problems and enable new applications more cost effectively. This section introduces a general framework to benefit from hyperspectral remote sensing by linking the analytical models of transportation systems analysis to outputs of the image analysis.

A first step in the general application of the framework is to identify the parameters of a transportation system model or aspects of the system that are directly observable using machine vision and analysis techniques. Numerous models already exist to study, estimate, and forecast the cost, performance, condition, safety, and security of multimodal and intermodal transportation networks. Existing approaches to estimate the values for observable model parameters require manual visual inspections or expensive terrestrial sensing equipment. Hyperspectral remote sensing using fleets of UASs has the ability and capacity to scale and provide cost-effective data collection platforms. Small and agile UASs are capable of capturing high spatial-spectral resolution scenes from transportation right-of-ways that include roadways, bridges, waterways, ports, pipelines, and railways.

The proliferation of high-speed wireless standards, low-power embedded computing, high-capacity memories, and cloud-computing platforms will continue to provide a steadily improving conduit for metadata data warehousing and analysis. These opportunities will continue to yield both rapid and cost-effective hyperspectral remote sensing and decision-support platforms. Therefore, transportation systems analysis would benefit from a change in paradigm by designing and developing new or improved models that are amenable to machine vision and image analysis methods or by modifying existing models that rely on terrestrial only data formats.

The ability to achieve rapid and wide area coverage with both high spatial and spectral resolution will enable numerous applications in multimodal and intermodal transportation capacity planning, environmental assessment, infrastructure monitoring, safety, and security. Capacity planning encompasses asset management, urban planning, travel demand forecasting, parking demand forecasting, corridor planning, and traffic analysis. Environmental assessment encompasses wetland identification, habitat protection, post-disaster management, and historical site assessment. Infrastructure condition and performance monitoring includes roadways, bridges, railways, terminals, pipelines, waterways, seaports, and airports. The area of transportation safety and security encompasses snow and ice detection and removal, toxic spill cleanup, law enforcement, hazard risk management, vulnerability assessment, and emergency response. Numerous parametric or empirical models are available to study and optimize the processes within each of these areas.

3.3 Scenario Studies and Results

The next sections will conduct three different scenario analyses in roadway congestion forecasting, railway condition monitoring, and pipeline risk management.

3.3.1 Roadway Congestion Forecasting

It is possible to use a flow-density model to forecast impending congestion for specific roadway types and geometries by measuring only the traffic density. Researchers still do not have precise closed form models to describe traffic flow and often turn to simulations that use empirical models. Congestion is largely a result of the interaction between vehicles that slow their speed. To understand how remote sensing can provide measurements that computers or planners can use to optimize traffic flow, this section derives the model of stable operating points.

It is convenient to analyze traffic flow in terms of spatial data representing a dynamic supply of vehicle gaps or time-headways along a segment or a bottleneck. The premise of this approach is that trailing distances are a function of speed because humans and computers need to account for reaction time, sight distances, and the deceleration achievable under prevailing conditions. Solving the equations of motion in terms of time-headway T_h yields volume V_p as the dependent variable where

$$V_p = \frac{T_h}{T_h^2 + T_r T_h - L_v / A_v} \quad (10)$$

T_r , A_v , and L_v are the reaction time, average vehicle deceleration, and the average length of a vehicle, respectively. This solution is most relevant to a freeway facility where the selected speed S_v is directly proportional to the achievable headway T_h such that

$$S_v = -A_v T_h. \quad (11)$$

Practically, speed selection depends on other factors. They include the speed limit and the presence of flow obstructions such as construction, incidents, and slow-moving vehicles in the traffic stream.

The average deceleration achievable also depends on the traffic mix and terrain. For example, the deceleration of a car will be lower if it must match that of a leading truck on a rural two-lane highway that has no passing zones. This analysis removes those constraints to determine the stable operating points in free- and forced-flow traffic.

Intuitively, time-headway extends the space that a vehicle occupies. Hence, as speed increases, vehicles eventually exhaust the available lane capacity. The time-headways are relatively small at slow speeds and this is why flow increases initially as speed increases. Eventually, the expanding time-headways begin to deplete capacity rapidly and become the dominant factor that actually decreases the vehicle flow rate. Manipulating the equations of motion and flow, and solving for volume as a function of density D yields

$$V_p(D) = \frac{1}{2} \left[\sqrt{A_v D (A_v T_r^2 D + 4 L_v D - 4)} + A_v T_r D \right] \quad (12)$$

Solving for the peak volume yields

$$V_{p\max} = \frac{A_v T_r + 2\sqrt{|A_v|L_v}}{A_v T_r^2 + 4L_v}. \quad (13)$$

The density D_{opt} at which the maximum volume occurs is

$$D_{opt} = \frac{2L_v - T_r\sqrt{|A_v|L_v}}{4L_v^2 + A_v L_v T_r^2}. \quad (14)$$

It is evident an optimum density that would maximize flow exists. Given the average length of a vehicle, the optimum density depends only on the average vehicle deceleration and driver reaction on that facility. Figure 3.1 plots this non-linear relationship for $L_v = 5.5$ meters, $A_v = -6.5 \text{ m/s}^2$, and $T_r = 0.66$ seconds.

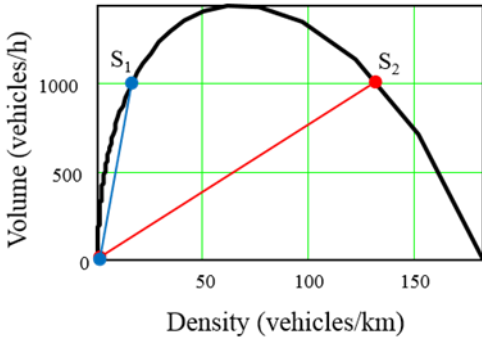


Figure 3.1 Theoretical Volume-Density Relationship

The same volume is achievable on either side of the peak value. However, the average speed will be higher in free-flow conditions, which are on the left side of the peak. Traffic transitions into forced-flow conditions as the density increases beyond the peak flow condition. The vehicle speed is the slope of a line from the origin to any point on the volume-density curve. For example, the volume is 1000 vehicles/hour for speed S_1 and S_2 but the density of vehicles is higher for the lower speed S_2 . This model assures that having an ability to identify and count vehicles in a remotely captured image will enable the accurate quantification of traffic density and hence the flow conditions.

The ability to identify vehicles from their spectral signatures is a mature field (Suzuki and Carrabba 2001), (McIntee 2008), and (Palenik, et al. 2014). The Digital Automotive Image System (DAIS) provides spatial information to identify vehicles manufactured within the past 20 years (NIST 2016). New “snapshot” hyperspectral sensors obtain a single spatial-spectral image within a few milliseconds (Lambrechts, Gonzalez, et al. 2014). Hence, they essentially eliminate speed-based distortions and the computational processing typically associated with a pushbroom type system.

3.3.2 Railway Condition Monitoring

Energy, or fuel consumption, is one of the largest factors in the cost of railroad operations, and it is an important consideration in route and locomotive selection. Several factors affect railroad energy

consumption. They include infrastructure and equipment related considerations. Infrastructure related factors include the line condition, degree of curvature, and the terrain type. Equipment related factors include the energy efficiency of locomotives and rolling resistance. The latter is a function of gross weight, speed, and aerodynamic factors. Remote sensing can help to characterize and catalog line segments of various degrees of curvatures, grades, and other conditions that impede rolling motion to validate existing energy consumption models, and to provide updated inputs to improve them.

A commonly used model for the force needed per ton of railroad car F_{RC} is (Armstrong 1990):

$$F_{RC} = R_R + 0.8D_R + 20G_R \quad (15)$$

where R_R is the rolling resistance on flat terrain, D_R is the degree of curvature, and G_R is the grade in percentage. All units are in pounds-per-ton (lb/ton). Various models exist that relate the flat-terrain rolling resistance to characteristics of the car. The Canadian National model is most applicable to modern cars that use roller bearings where:

$$R_R = 1.5 + \frac{18N_{AC}}{W_C} + 0.03V_R + \frac{c_{dr}a_{cr}}{10000 \cdot W_C} V_R^2 \quad (16)$$

The first two terms represent the speed-independent resistance, which is a function of track quality and bearing resistance, the number of axles N_{AC} , and the total weight of the car W_C in tons. The third term is dependent on the vehicle speed V_R (mph) where the resistance is a function mostly of wheel-rail interface factors such as flange friction, dynamic flange motion, and wheel resistance. The last term is also speed-dependent; it includes a streamlining coefficient c_{dr} and the frontal car area a_{cr} to account for aerodynamic effects such as air pressure, rear drag, and air turbulence.

The high spectral contrast of metal rails and the intervening material such as ballast, soil, and vegetation makes it possible to assess the uniformity of line quality. Uneven wear and rusting will produce variations in their spectral signature to indicate changes in rolling resistance. Irregular spatial geometry on flat terrain such as buckling, kinks, cracks, and railhead abrasions can impede smooth rolling motion. UAS-based hyperspectral systems with resolution agile snapshot sensors provide a method of simultaneously acquiring images at both the spectral and spatial resolutions needed. Such platforms have the ability to zoom adaptively and obtain higher spatial resolution of target areas within a small field of view. The ability to assess these conditions could provide inputs for improving the rolling resistance model and augment maintenance information to improve railroad safety. The energy required for any route is directly proportional to the sum of forces needed to move the train along various portions of the track having different combinations of rolling resistance, curvature, grade, and speed limit.

3.3.3 Pipeline Risk Management

The visual identification of toxic spills along pipeline rights-of-way can be nearly impossible because of their changing appearance over time and the limited accessibility of those environments. Fortuitously, the characteristically strong reflectance features of toxic materials such as hydrocarbons and brine make hyperspectral techniques suitable for their detection (Salem and Kafatos 2001). Infrared remote sensing has proven effective in the detection of oil spills on open water (Warren, et al. 2014). The combination of hydrocarbon absorption peaks provides unique signatures for the early detection of spills and the subsequent monitoring of cleanup efforts. The ability to classify hyperspectral scenes in real time will provide navigational adaptability to guide UAS-based imagers to suspected spill areas for higher resolution image acquisition. However, the computational complexity of existing high performance classifiers limits their ability to provide real-time results (Borengasser, Hungate and Watkins 2010).

This research introduces a simple spectral classifier (SSC) to demonstrate the separability in feature space of hydrocarbon materials from other forms of ground cover. Figure 3.2 displays the SSC feature space for selected materials sampled from endmembers of the NASA Advanced Spaceborne Thermal Emission Reflection Radiometer (ASTER) Spectral Library (Baldrige, et al. 2009).

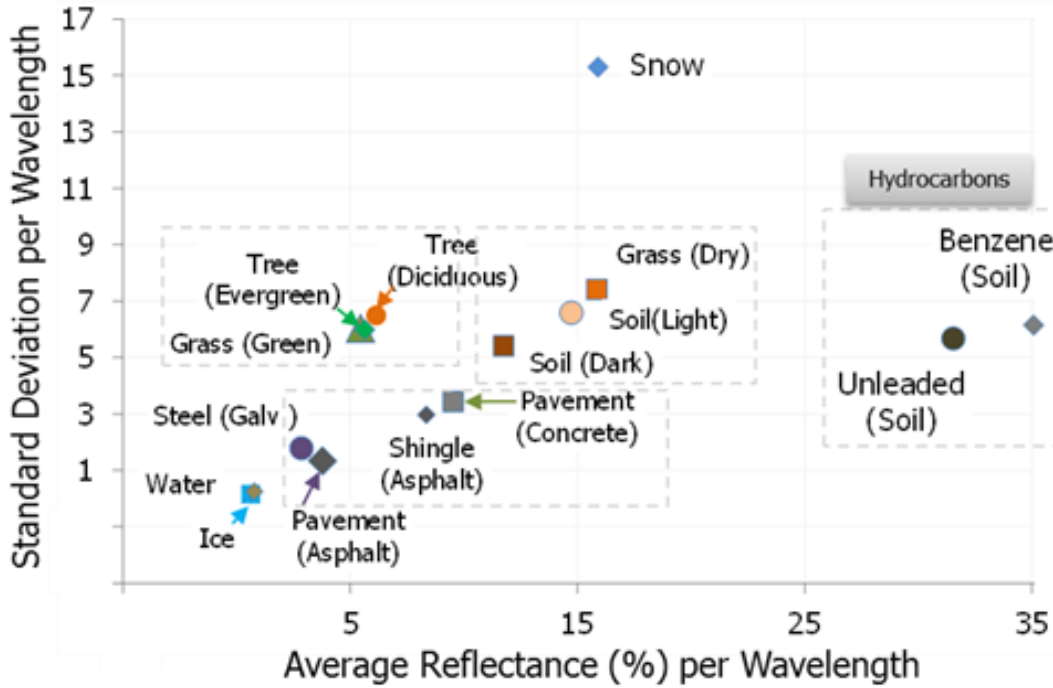


Figure 3.2 The SSC Feature Space for Selected Materials

The SSC incorporates the bandwidth normalized albedo and standard deviation of endmember spectral signatures to create a simple two dimensional classification space. The standard deviation σ_g of the reflectance spectra is

$$\sigma_g = \sqrt{\frac{1}{N} \sum_{n=1}^N (g_n - \mu_g)^2} \quad (17)$$

where the mean reflectance percentage or albedo μ_g is

$$\mu_g = \frac{1}{N} \sum_{n=1}^N g_n. \quad (18)$$

The reflectance percentage in spectral band n is g_n and the wavelength-normalized albedo (AVN) is

$$AVN = \frac{\mu_g}{\lambda_H - \lambda_L} \quad (19)$$

where λ_H and λ_L are the highest and lowest wavelength bands, respectively. Similarly, the wavelength-normalized standard deviation (SDN) is

$$SDN = \frac{\sigma_g}{\lambda_H - \lambda_L} \quad (20)$$

The physical meaning of the AVN is the reflective nature of a material per unit of wavelength across the spectral region of interest. The SDN is a measure of the overall variations in reflectivity of a material per unit of wavelength. The SSC feature space naturally organizes these materials into the six classes shown in the figure. The classes are aquatic, living organics, dry organics, manufactured surfaces, snow, and hydrocarbons. These materials represent a majority of the ground cover in and around typical transportation infrastructures.

At small zenith angles, aquatic materials are highly absorptive throughout the spectral region. This characteristic places the ice and water spectra at an extreme corner of the feature space. Conversely, snow is highly reflective in the visible region and varies in albedo at longer wavelengths. Those features place it in the upper portion of the feature space.

The measure of separability is the Euclidian distance proportion of the maximum distance in the normalized feature space. The Euclidian distance proportion D_η is

$$D_\eta = \frac{1}{D_{max}} \sqrt{(g_{nx} - h_{nx})^2 + (g_{ny} - h_{ny})^2} \quad (21)$$

where D_{max} is the maximum Euclidean distance for all features in the normalized space, \mathbf{g} and \mathbf{h} are vectors of the extracted features for any two materials, x and y are the scaled feature space vector components for the horizontal and vertical axis, respectively.

The average separability for hydrocarbons from the other material classes is 43.4%. Excluding the outlier materials of hydrocarbons and snow to remove the bias provides an average inter-class separability of 22.1%, which is still relatively high. The average intra-class separability, however, is only 3.3%. This result demonstrates that hydrocarbons separate reasonably well from the other classes. However, an improved ability to distinguish amongst materials of the same class would likely require a more computational complex algorithm.

This scenario demonstrates the potential for the real-time detection of hazardous spills containing high hydrocarbon and water content by using simple but effective classifiers that offer ample separability between material classes.

3.4 Section Conclusion

The primary benefit derived from using hyperspectral remote sensing to characterize the global transportation infrastructure is the simultaneous spatial and spectral information that it provides about the targets. Typical models of transportation systems analysis utilize information only from the spatial and temporal domains. This study introduced a generalized framework for the utilization of both spatial and spectral data to improve and enable many applications in transportation systems. The authors demonstrated the framework within three specific areas where hyperspectral remote sensing provided an appropriate approach to quantify the identified parameters. Table 3.1 summarizes their expert assessment of conservative spatial and spectral capabilities needed for the three application areas analyzed.

Table 3.1 Typical Spatial and Spectral Requirements

Application Resolution Requirements	Roadway Congestion Monitoring	Railway Condition Monitoring	Pipeline Risk Assessment
Spatial	1 m	5 cm	1 m
Spectral	15 bands 10 nm/band	12 bands 10 nm/band	4 bands 50 nm

Implementation difficulties such as sensor cost, instrumental complexity, payload weight, data archiving, rapid image analysis, and high latencies in the data decision framework are rapidly diminishing. The authors have recently acquired a UAS with procurement procedures in place to accept delivery of a hyperspectral mosaic sensor. The team is currently planning to conduct field-based observations relevant to these three topics. Hyperspectral remote sensing will lead to a paradigm shift in transportation systems modeling.

4. PART III – FRAMEWORK APPLICATION FOR HAZARDOUS SPILL DETECTION

This section demonstrates additional details in using the hyperspectral remote sensing framework developed in the previous sections. It further explores application of the framework to develop a model to manage pipeline risks, particularly the rapid detection of hazardous spills.

4.1 Section Introduction

Sustained growth in industrial and commercial activities that rely on hazardous material transport increases the risks of hazardous material spills. Government studies indicate that traffic carrying flammable, corrosive, poisonous, and radioactive materials exceed 800,000 shipments per day (Craft 2004). A case study of crude oil transport demonstrates that spills from pipelines, trains, and commercial motor vehicles pose a serious threat to public safety (USDOT 2015). The release of hazardous materials often results in environmental contamination and property damage that cost millions of dollars and years to remediate (GAO 2014). Corrosion is a leading cause of pipeline failures (USDOT 2011). Hence, the risk of future accidents increases with pipeline aging. Currently, the age of more than 70% of the crude oil pipelines in the U.S. exceeds 45 years. The lack of pipeline capacity has led to a factor of 24 increase in rail carloads from 2008 to 2012 (GAO 2014). This ramp in rail traffic has raised new concerns about testing and packaging. In the United States, there are more than 630,000 miles of hazardous liquid gathering and transmission pipelines, and more than 140,000 miles of railroad (USDOT 2011). Many miles of the pipeline and railroad rights-of-way pass through populated and environmentally sensitive areas.

The lack of regular ground inspections and systems to detect hazardous material releases result in missed detections. A government study found that the public generally reports pipeline leaks quicker than company installed sensors (Kiefner & Associates, Inc. 2012). Operators cannot easily inspect buried pipes, and rugged terrain often precludes ground inspections (Kiefner & Associates, Inc. 2012). Remote sensing using spaceborne and airborne platforms offer the potential to monitor large areas for hazardous material spills quickly and regularly (Bridgelall, Rafert and Tolliver, Hyperspectral Imaging Utility for Transportation Systems 2015). Hyperspectral image sensors add a spectral dimension to enhance sensitivity and reduce missed detections (Bridgelall 2014). However, high-altitude platforms limit the spatial resolution needed to preclude false positives. The emergence of small, rotary and fixed-wing, unmanned aircraft systems (UASs) offer the potential for resolution agile platforms. Their ability to trade-off mobility and accessibility while flying enables the possibility of validating potential targets in real time. Pilots or autopilot algorithms can adapt sensor parameters and/or maneuver the aircraft to obtain higher resolution images of select target areas. However, real-time adaptation requires a method of rapid hyperspectral image classification to provide operators or algorithms with the data needed to make decisions while navigating.

The computing capacity that existing methods of hyperspectral image classification need to match the typical rate of image acquisition is impractically large. The desired combination of high computational capacities, low power consumption, and low cost is not yet available for integration with UASs (Bridgelall, Rafert and Tolliver 2015). Methods of hyperspectral image classification vary in performance and computational complexity as a function of the available spatial and spectral resolutions. An increase in the onboard processing requirement typically leads to a more rapid depletion of the energy available for flight endurance. The limited wireless bandwidth and communications range available also precludes the real-time transmission of hyperspectral data to a remote processor.

The objective of this research is to develop a method of rapid hyperspectral image classification that can detect anomalous materials such as hydrocarbon spills with performance levels that approach the prevailing methods. The organization of this paper is as follows: the next section will provide a background on the existing methods of hyperspectral image classification and their computational complexities. The third section will develop the methods and models of rapid feature extraction and classification. The fourth section will assess the performance of the method using two criteria and provide case studies of each. The final section will summarize and conclude the research.

4.2 Background

Noise and distortions from the data collection apparatus and the large path lengths through the atmosphere corrupt reflectance values. Furthermore, contamination such as dirt, vegetation, and water distorts the spectral signature of a pure target material such as hydrocarbons. Classification methods, therefore, attempt to assign every hyper-pixel to a class of materials based on some measure of similarity. Current methods of hyperspectral image classification fall into two categories: supervised or unsupervised (Mather and Tso 2003). The former requires a training set or a library of endmembers to determine each pixel assignment based on similarities of their characteristics. Unsupervised methods preclude training requirements by forming clusters of closely related hyper-pixels.

Methods of unsupervised classification, such as principle component analysis (PCA), independent component analysis (ICA), and singular value decomposition (SVD), identify at least one orthogonal feature set in the hyperspectral scene. However, they are at least $O(PN^2+N^3)$ computationally complex (Du and Fowler 2008). Here, P is the number of hyper-pixels and N is the number of spectral bands. An important shortcoming is that new orthogonal features generally do not provide a clear physical meaning for data interpretation and decision-making (Prats-Montalbán, Juan and Ferrer 2011). Algorithms such as the Iterative Self-Organizing Data Analysis Technique (ISODATA) assign hyper-pixels with similar characteristics into clusters. The iterative procedure is very sensitive to the number and types of initial features selected. Convergence depends on the heuristics of setting a threshold for the number of endmember reassignments. Such algorithms are $O(PKN^2I)$ complex where K is the number of clusters, and I is the number of iterations (Tarabalka, Benediktsson and Chanussot 2009). To minimize their computational complexity, analysts typically incorporate methods of feature selection to identify a minimum number of subset bands that would maintain some measure of sufficiency in class separability. However, the feature selection algorithms themselves typically have $O(PN^K)$ complexity (Bajcsy and Groves 2004).

Supervised methods assign each hyper-pixel to one of several user-defined classes based on a measure of similarity to members of each class. Spectral similarity measures include both statistical and machine learning methods. The statistical methods most often used are Spectral Angle Mapper (SAM), Minimum Distance Classifier (MDC), Maximum-Likelihood Classifier (MLC), Spectral Information Divergence (SID), and Spectral Correlation Mapper (SCM). The SAM is by far the most popular method (Homayouni and Roux 2004). The computationally complexities of the prevailing supervised methods range from $O(N^2)$ to $O(N^3)$. The literature lacks algorithms that are significantly less computationally complex.

4.3 Method of Rapid Classification

The method of rapid classification described in this research is a hybrid supervised-unsupervised technique. The unsupervised aspect is a feature extraction method that operates once on every new hyper-pixel and library endmember. The supervised aspect is a comparison of feature sets that uses either radial cell or rectangular quadrant assignments in a two-dimensional (2-D) feature space. The feature extraction for library endmembers is precomputed. Hence, it could occupy a much smaller amount of digital

memory within onboard computers. The reduced computational complexities of one-time feature extraction per new hyper-pixel, and the simpler similarity comparisons with endmembers enable the potential for real-time classification. For equidistant endmembers, the assignment will be the same as that of the nearest hyper-pixel neighbor that does not have an ambiguous assignment to the same set of equidistant endmembers.

4.3.1 Feature Extraction

The typical spectral library contains a list of endmembers represented as atmosphere corrected albedo values for each spectral band available (Figure 4.1). The albedo is a measure of the portion of incident solar energy reflected from a material. NASA's earth observation satellites regularly measure and report the average albedo of the earth's surface in the visible wavelength ranges. This value has been about 30% (Richards 1999). The typical ground cover materials of remote areas include various types of vegetation and bare soil (Baldrige, et al. 2009). The overall shape of each endmember will be unique with sufficient spectral resolution and bandwidth. The *selectivity* of the approach, which is an ability to discern among different materials, improves with greater spatial and spectral resolutions. A unique advantage of UASs is the ability to enhance spatial resolution and signal quality by moving the sensor closer to the target. This resolution agile capability will enhance the quality of images within the *sensitivity* range of the system to detect lower spill concentrations among contaminating materials.

One of the simplest features often extracted is the average albedo. Related efforts used the average albedo to estimate the age of asphalt pavements (Herold, et al. 2008), to identify snow-cover, and to track waterways in real-time (Clark, et al. 2010). This research modifies the average albedo and defines another statistical feature to form a simple 2-D feature space.

The Wavelength Normalized Average Albedo (AVN)

The average albedo μ_g and the wavelength normalized average albedo (AVN) is provided by Equation (18) and (19), respectively, in the previous section. The normalization per wavelength band facilitates comparisons between endmembers with different spectral resolutions and bandwidths, potentially from combining different libraries. Hence, normalization accommodates band selection methods that attempt to eliminate wavelength channels that do not appreciably decrease the separability between a subset of endmembers targeted to a specific application. A similarly modified feature is the normalized standard deviation (SDN) defined previously. The pair of extracted features {AVN, SDN} provides a low complexity feature space that establishes the separability amongst endmember classes.

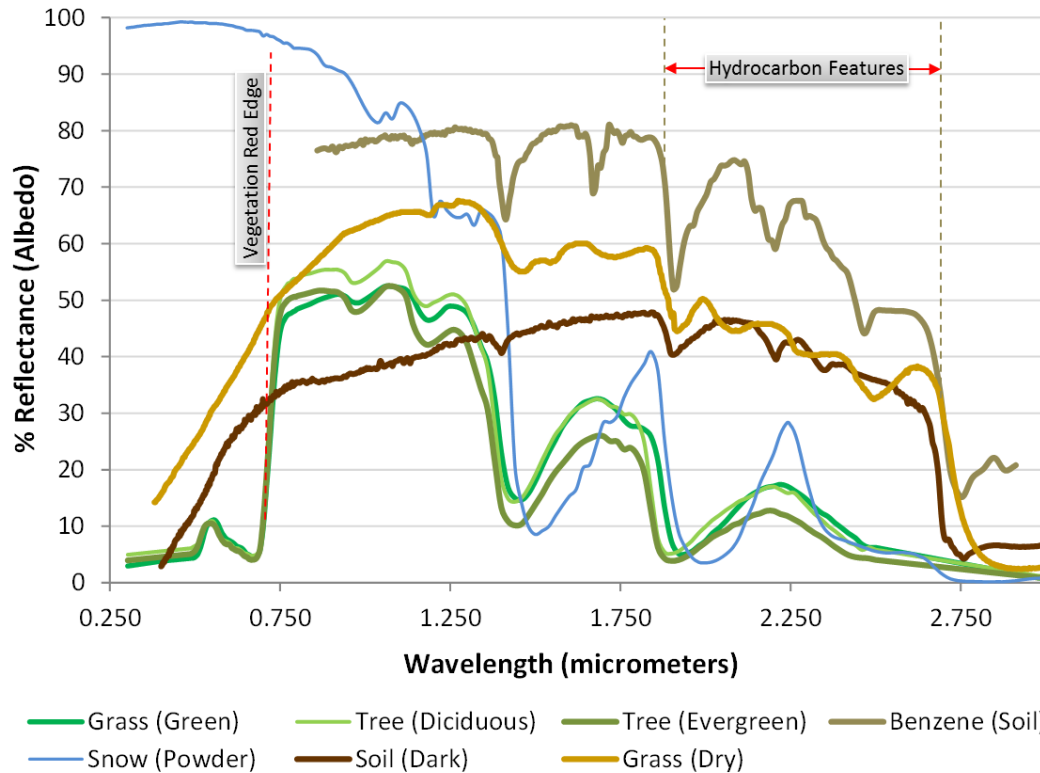


Figure 4.1 Spectral Signatures for Typical Ground Cover

The Wavelength Normalized Standard Deviation (SDN)

To diversify the feature space, the SDN characterizes the variability of a spectral signature. The standard deviation σ_g of the reflectance spectra is provided by Equation (17) in the previous section. The SDN is provided previously by Equation (20). As mentioned previously, division by the spectrum bandwidth normalizes the variations across the available spectral ranges of library endmembers. The physical meaning of the AVN is the reflective nature of a material per unit of wavelength across the spectral region of interest, whereas the SDN is a measure of the overall variations in reflectivity of a material per unit of wavelength.

4.3.2 Distance Measure

The simple spectral classifier (SSC) computes a pair of {AVN, SDN} feature for each hyper-pixel of the acquired image frame and compares their distance with each target endmember. For a given spatial and spectral resolution, the level of reflectance noise and material contamination of the target will proportionately increase the feature space distance between the captured signature and the signature of the corresponding library endmember. Therefore, a feature space that exhibits relatively large separation distances among endmember combinations will accommodate a greater level of target noise and contamination while maintaining its association with the endmember class of materials. Subsequently, an ability to compare the average separability of selected endmembers in their respective classifier feature spaces establishes an effective approach to compare their relative potential for generating false positives. This approach is a first step that precludes the enormous expense of conducting extensive field experiments to compare actual false positive rates among different classifiers.

As mentioned previously, the SSC uses the Euclidian distance proportion of the maximum distance in the normalized feature space as the measure of separability. The Euclidian or radial distance proportion D_{η} is provided by Equation (21) of the previous section. The SDN feature space is scaled to equal the dynamic range of the AVN feature space.

The SSC feature space for 15 typical ground cover materials organizes into six macro-classes of materials (Figure 3.2). Members of the same class have similar spectral signatures. Hence, the average separability among intra-class signatures is substantially less than the average separability among inter-class members. At small zenith angles, materials of the aquatic class are highly absorptive throughout the spectral region. This characteristic places water and ice at an extreme lower corner of the feature space. Conversely, snow of different consistency is typically highly reflective in the visible region and varies in albedo at longer wavelengths. Those features place it near the top of the feature space. The hydrocarbon endmembers shown in the feature space are relatively small concentrations of benzene or unleaded gasoline mixed with clay (Baldrige, et al. 2009). The hydrocarbons exhibit a combination of high average reflectivity and medium variability in albedo that places it at the extreme right corner of the SSC feature space.

By inspection, the SSC separates hydrocarbons and snow reasonably well from the other materials so that they appear as outliers in the feature space. Conversely, intra-class materials such as evergreen trees and green grass exhibit less separability. Hence, applications that need to distinguish among intra-class similar materials will likely require a different type of classifier that features a higher average separability but likely more computationally complex. This limitation of the SSC points to a trade-off in computational complexity and intra-class separability. Consequently, the rapid classification capability of the SSC will be most suitable for applications that seek to identify anomalies in a scene for further scrutiny. For example, oil spilled from a pipeline onto a vegetation or soil patch will likely exhibit obvious and abrupt changes in the SSC material classes. Subsequently, the appropriate use of UASs will provide a resolution agile capability for closer inspection and validation.

4.4 Results and Discussions

The two key performance measures are the average separability of endmembers in the new feature space and the computational complexity of the new classifier. The separability analysis will use the materials sampled from the ASTER Spectral Library (Baldrige, et al. 2009). A case study of the separability performance will compare the relative distances between endmember combinations in the SSC and the SAM feature spaces. Comparing the actual computational resource needs of several classification methods will require a new benchmark that is appropriate for computer architectures that manufacturers optimize to process images at high speed. A case study of the computational complexity using state-of-the-art mobile image processors will quantify the trade-off in processing needs and image classification speed.

4.4.1 Separability Performance

The average feature-space distance between the same combinations of inter- and intra-class endmember samples provides a means to compare the relative separability of different classifiers. Table 4.1 shows the separability for materials in the denser cluster near the center of the feature space as a proportion of the maximum SSC feature space distance (cell entries 'na' mean not applicable.) This comparison excludes the outlier clusters such as hydrocarbons and snow to remove bias in the separability assessment. This combination also simplifies the table to a more meaningful set of materials for ease of visualization and clarity. Hence, these endmember samples from the large spectral library will serve as the standard to compare the SSC separability with other classifiers.

Table 4.1 SSC Separability Matrix for Typical Ground Cover

	Soil (Dark)	Tree (Con)	Tree (Dec)	Concrete	Ice
Soil (Light)	8.0%	18.9%	17.3%	17.4%	40.3%
Grass (Green)	na	0.4%	2.4%	13.7%	27.8%
Tree (Conifer)	na	na	2.4%	14.1%	27.8%
Shingle (Asphalt)	na	na	na	3.2%	20.0%
Pavement (Concrete)	na	na	na	na	23.2%

The average separability for the selected materials is 15.8%. The inter-class separability (highlighted cells) is 22.1%. whereas the intra-class separability is 3.3%. Borrowing from the interpretation of chi-squared statistics goodness-of-fit testing that uses a 5% significance threshold, a candidate signature is not likely a member of the tested class if its separability is greater than 5%. Therefore, the greater than 10% separability among different classes qualifies the SSC performance to identify materials that are likely contaminants or anomalies, e.g., oil spills that do not naturally occur within vegetation, top soil, or aquatic bodies. However, the less than 5% intra-class separability indicates that this method may not be as suitable for distinguishing among materials with similar signatures.

Case Study of Relative Separability

The SAM is one of the most popular techniques for quantifying the separability of spectra in feature spaces (Meer, et al. 2012). The model represents spectra as a vector in N-dimensional space and computes the “angle” between vectors as the measure of similarity. The SAM maps the separation of two vectors in multidimensional space to an angle α_s in degrees such that

$$\alpha_s = \arccos \left(\frac{\sum_{n=1}^N f_n g_n}{\sqrt{\sum_{n=1}^N f_n^2 \sum_{n=1}^N g_n^2}} \right) \quad (22)$$

where f is the spectrum of a hyper-pixel, g is the reference spectrum, and n is the index of the wavelength band (Sohn and Rebello 2002). It is evident that for identical hyper-pixels where $f = g$ the expression evaluates to zero degrees. This approach requires that the compared spectra have matching spectral bands. Of the material combinations analyzed in this study, only six were comparable using the SAM. It is possible to resample spectra to equalize their wavelength bands, but resampling introduces errors that distort the results of the feature extraction methods.

The proportional SAM distances for the available combinations are the angle of separation as a percentage of the maximum separation angle in the feature space, which is 90 degrees (Table 4.2). The average SAM separability improvement over the SSC for this sample of library endmembers is 7.2%. This comparison focused on the materials in the center cluster of the SSC space and excluded the outliers such as hydrocarbons and snow. Therefore, the less than 10% improvement of the SAM over the SSC for materials with signatures that are more similar indicates that both would be similarly effective. Moreover, this result also indicates the potential effectiveness of the SSC classifier in identifying anomalies such as hydrocarbons.

Table 4.2 Class Separability for SAM and SSC

Class Separability	SAM	SSC	Difference
Soil (Light) – Soil (Dark)	17.2%	8.0%	9.2%
Grass (Green) – Tree (Deciduous)	8.0%	0.4%	7.6%
Tree (Evergreen) – Tree (Deciduous)	4.1%	2.4%	1.7%
Shingle (Asphalt) – Concrete	16.2%	3.2%	13.0%
Shingle (Asphalt) – Ice	25.8%	20.0%	5.8%
Concrete – Ice	29.1%	23.2%	5.9%
AVERAGE	16.7%	9.5%	7.2%

4.4.2 Computational Complexity

This study defines the multiply-accumulate complexity (MACC), denoted $\Pi[D]$ where D is the number of clock cycles that a model requires when implemented on processors capable of single-cycle multiple-accumulate (MAC) operations. The typical digital signal processor (DSP) and some alternative architectures optimized for mobile devices implement a MAC operation within a single instruction cycle. However, they implement divisions using a series of bit shifting and comparison operations that amount to approximately 42 clock cycles for a 32-bit signed division (Cheng 2000). The MACC notation is more convenient than the Big-O notation to benchmark the computing time on processors optimized for signal and image processing. As is customary with the Big-O notation, the MACC ignores operations that do not include multiplications, such as additions or comparisons (subtractions). The MACC also excludes divisions and multiplications by integer constants that are powers of two because DSPs can calculate those using single-cycle bit-shifting operations that consume negligible resources. Additionally, the MACC excludes operations that algorithms can precompute and store in memory for later use. For instance, algorithms can precompute operations that involve only library endmembers. Furthermore, the MACC excludes computations that operations can store from previous cycles of an iteration.

Spectral Angle Mapper (SAM)

The SAM has a MAC complexity of $3\Pi[N]$ operations plus one square root, one division, and one arccosine operation. The Taylor series expansion for a square root operation provides the baseline for estimating the number of MAC operations where (Thomas and Finney 1995):

$$\sqrt{1+z} = 1 + \sum_{k=1}^C \frac{(-1)^k (2k)!}{4^k (k!)^2 (1-2k)} z^k \quad (23)$$

The selection of C provides the desired precision. The exponential and factorial operations of each iteration can use extra memory to precompute and store the results for future iterations. The exponent of the argument z requires $\Pi[C]$ operations by storing the results from previous iterations. Multiplication with the precomputed constants of each iteration requires one additional MAC. Therefore, the MACC of the square root operation is $2\Pi[C]$.

The Maclaurin series expansion for the arccosine of the argument z is (Thomas and Finney 1995):

$$\arccos(z) = \frac{\pi}{2} - \sum_{k=1}^C \frac{(2k)!}{4^k (k!)^2 (2k+1)} z^{2k+1} \quad (24)$$

In a manner similar to the square root operation, precomputing the constants will reduce the iterative computational requirements. The exponential operation requires $\Pi[2C + 1]$ and multiplication by the constant in each iteration will require one additional operation. Hence, the MACC of the arccosine operation is $2\Pi[2C + 1]$. Therefore, the total MAC complexity of the SAM classifier per image frame of P hyper-pixels is

$$\Pi_{\text{SAM}} = P \times K \times \{\Pi[3N] + \Pi[8C] + \Pi[44]\}. \quad (25)$$

Bhattacharya Distance (B-Distance)

The Bhattacharya Distance (B-Distance) and the Maximum Likelihood Classifier (MLC) are two other frequently utilized classifiers. The B-distance is an index that is proportional to the amount of overlap between two probability density functions $f(x)$ and $g(x)$ of hyper-pixel vector \mathbf{x} (Landgrebe 2002). For Gaussian density functions, the model is

$$B = \frac{1}{4} \ln \left[\frac{1}{4} \left(\frac{\sigma_f^2}{\sigma_g^2} + \frac{\sigma_g^2}{\sigma_f^2} + 2 \right) \right] + \frac{1}{4} \left(\frac{(\mu_f - \mu_g)^2}{\sigma_f^2 + \sigma_g^2} \right) \quad (26)$$

where σ_f and σ_g are the standard deviations of the first and second spectra, respectively, and μ_f and μ_g are the means of the first and second spectra, respectively. Each variance requires $\Pi[N + 1]$ operations. The series expansion for a logarithm operation is (Thomas and Finney 1995):

$$\ln(z) = \sum_{n=0}^{\infty} \frac{(-1)^n}{n+1} (z-1)^{n+1} \quad (27)$$

By inspection, the logarithm operation requires $2\Pi[C + 1]$ MAC cycles. Therefore, the total MACC of the B-Distance per image frame of P hyper-pixels is

$$\Pi_{\text{B-dist}} = P \times K \times \{2\Pi[N + 1] + 2\Pi[C + 1] + \Pi[172]\}. \quad (28)$$

Maximum Likelihood Classifier (MLC)

The MLC estimates the probability $g_i(x)$ that an observed hyper-pixel \mathbf{x} belongs to a predetermined spectral class ω_i of the i^{th} class in the scene such that

$$g_i(x) = \ln p(\omega_i) - \frac{1}{2} \ln |\Omega_i| - \frac{1}{2} [\mathbf{x} - \boldsymbol{\mu}_i]^T \Omega_i^{-1} [\mathbf{x} - \boldsymbol{\mu}_i] \quad (29)$$

where $p(\omega_i)$ is the probability that spectral class ω_i is present in the scene (Richards 1999); $|\Omega_i|$ is the determinant of the covariance matrix for the group of spectra in class ω_i ; Ω_i^{-1} is the inverse of the covariance matrix; $\boldsymbol{\mu}_i$ is the mean vector for the group of spectra in class ω_i . MLC implementations may precompute the matrix determinants and inversions for each target class; hence, the MACC does not include them. Furthermore, the first term to determine the probability of class presence in a scene is done only once for each class endmember. This procedure requires calculating at least a variance for each hyper-pixel that will require at least $\Pi[(N + 1)P]$ operations, plus the final natural logarithm. The final set of matrix operations will require at least $\Pi[2N]$ operations for a single endmember representing a class.

The division by 2 is a right-shift operation, so the MACC does not include it. Therefore, the total MACC of the MLC per image frame of P hyper-pixels is

$$\Pi_{\text{MLC}} = P \times K \times \Pi[2N] + \Pi[P(N + 1)] + 2\Pi[C + 1]. \quad (30)$$

Wavelength Normalized Standard Deviation

Computing SDN requires $\Pi[N] + \Pi[1] + 2\Pi[C]$ MAC cycles. The wavelength ratios are precomputed. The AVN requires $\Pi[2]$. The SSC operates on each of the P hyper-pixels only once to determine their {AVN, SDN} coordinate. The SSC assigns each coordinate to the class having the minimum Euclidian distance. There are $P \times K$ Euclidian distance calculations that require $2\Pi[C] + \Pi[3]$ MAC cycles. Therefore, the one-time SSC computation per hyper-pixel and the assignment to a class requires $P \times \{\Pi[N] + 2\Pi[C] + \Pi[3]\}$ and $P \times K \times \{2\Pi[C] + \Pi[3]\}$ operations, respectively. Therefore, the total MACC of the SSC classifier is

$$\Pi_{\text{SSC}} = P \times K \times \{2\Pi[C] + \Pi[3]\} + P \times \{\Pi[N] + 2\Pi[C] + \Pi[3]\}. \quad (31)$$

Assigning SSC features to a rectangular quadrant of the feature space would reduce the complexity further by requiring only $P \times K$ subtraction operations. This would yield a SSC-Rectangular (SSC-R) classifier that has a complexity of

$$\Pi_{\text{SSC-R}} = P \times 1 \times \{\Pi[N] + 2\Pi[C] + \Pi[3]\}. \quad (32)$$

Case Study of Computational Complexity

As of 2015, the Airborne Visible/Infrared Imaging Spectrometer (AVIRIS) sensor has been the most popular platform for airborne hyperspectral image acquisition. It provides $N = 224$ spectral channels that range from 360 to 2500 nanometers (Coulter, Hauff and Kerby 2007). When aboard a Twin-Otter aircraft at an altitude of 4 km, the AVIRIS provides a spatial resolution of 4 meters. Hence, there will be $P = 62,500$ hyper-pixels per square-kilometer of the scene. Although a typical application will tend to classify materials into dozens of classes, this case study will use the $K = 15$ material types shown for the SSC as prototype endmembers for a class. The highest exponent of the polynomial in the series expansion should be at least $C = 3$ when computing the arccosine, logarithm, and square root functions with at least one significant digit of accuracy (Muller 2006). To summarize, the parameters for the case study are $P = 62,500$, $N = 224$, $C = 3$, and $K = 15$.

The processing requirements computed are per square-kilometer of hyperspectral scenes collected with the AVIRIS Twin Otter system (Table 4.3). For this scenario, the number of classifications per frame is PK, which totals 937,500. The third and fourth columns list the number of MAC operations per classification (Π s/PK) and the total MACs per frame (Total Π s), respectively. It is evident that the SAM requires 30 and 48 times more processing capacity than the SSC and the SSC-R, respectively.

Table 4.3 Relative Complexities of the Classifiers

Model	Computational Cost Model	PIs/PK	Total PIs	Time (s)
SAM	$P \times K \times \{\Pi[3N] + \Pi[8C] + \Pi[44]\}$	740	694M	53.4
B-Distance	$P \times K \times \{\Pi[2(N+1)] + \Pi[2(C+1)] + \Pi[172]\}$	630	591M	45.4
MLC	$P \times K \times \{\Pi[2N] + \Pi[P(N+1)] + \Pi[2(C+1)]\}$	463	434M	33.4
SSC	$P \times K \times \{\Pi[2C] + \Pi[3]\} + P \times \{\Pi[N] + \Pi[2C] + \Pi[3]\}$	25	23M	1.8
SSC-R	$P \times 1 \times \{\Pi[N] + \Pi[2C] + \Pi[3]\}$	16	15M	1.1

The last column of Table 4.3 lists the execution time for each method for a processor that can allocate 13 million multiply-accumulate cycles per second (MMACS) of capacity. The latest generation of mobile computers has approximately 400 MMACS of total processing capacity (Cole 2014). Hence, the SSC will consume 3% of that capacity, whereas the SAM would require 98% of it to classify scenes at the same rate. The SSC and the SSC-R processing speeds shown will support image acquisition rates greater than 0.5 square-kilometers per second. The AVIRIS Twin-Otter can capture hyperspectral images at a maximum rate of approximately 0.4 square-kilometers per second (Coulter, Hauff and Kerby 2007). Therefore, UAS platforms capable of similar image acquisition rates can perform real-time classification of hyperspectral images using the SSC and SSC-R and only 3% of the processing capacity of state-of-the-art mobile computing platforms.

4.4.3 Considerations for Transfer to Practice

The first step in transfer to practice requires the regulatory approval for a suitable UAS platform and its hyperspectral camera payload. Subsequently, practitioners must implement the SSC classifier on the existing single-board computer of the UAS, or design the algorithms to execute on a separate computing module dedicated to image classification tasks. The precomputed SSC feature space of the library endmembers must include at least their pair of extracted features {AVN, SDN}. The dedicated computing module or memory space of the single onboard computer may store the compressed endmember library of the SSC feature space. The classification tasks must communicate the results of real-time classification to the control module that implements operating and navigational response rules. Alternatively, the classification tasks may transmit classification results for real-time display to the remote pilot who is controlling the UAS. Therefore, the UAS may adjust its navigation autonomously or under remote pilot control to approach potential targets for more detailed scrutiny and verification.

4.5 Section Conclusions

Remote sensing using small and agile UASs has the capacity to scan large ground areas rapidly. The ability to adapt flight altitudes and speeds continuously enables real-time searches by trading off area coverage for higher image resolution while flying. Remote pilots or onboard algorithms can navigate to potential targets discovered within large swaths by swooping down or zooming in to obtain images at higher spatial resolution for further scrutiny. Such a resolution agile system will enable verifications of hazardous material spills in real time to reduce or eliminate false positives. Hyperspectral imaging adds high spectral resolution to enhance the sensitivity of target detections. However, hyperspectral imaging comes at the price of large data cubes per image frame. The high processing capacity needed to classify hyperspectral images poses significant challenges when using low-power mobile computing platforms. This limitation often precludes their use aboard small and agile unmanned aircraft systems (UASs).

This research developed a method of rapid hyperspectral image classification that enables real-time navigational guidance based on target materials detected in the scene. The approach is a hybrid supervised-unsupervised technique that extracts simple statistical features of the spectra for comparison with target endmembers. The statistical features are a wavelength-normalized average albedo (AVN) and a wavelength normalized standard deviation (SDN). Together, the pair of extracted features establishes a

simple two-dimensional (2D) feature space. This enables the simple spectral classifier (SSC) to perform a Euclidian distance or quadrant comparison between each hyper-pixel and target endmember. The simple features facilitate pre-compression of the spectral library of target materials to result in several-fold reduction of onboard computer memory requirements.

Separability analysis demonstrates that the SSC provides approximately 16% separation among library endmembers that composes a majority of ground cover materials, including hydrocarbons. Prevailing algorithms such as the spectral angle mapper (SAM) provide a modest improvement in separability of 7.2% for materials in tight clusters of the SSC feature space. However, the SSC is less capable of separating materials with similar signatures.

This research developed a method to benchmark the computational speed of classifiers on computer architectures that manufacturers optimize for mobile image processing. The analysis reveals that the SAM requires at least 30 times more processing capacity than the SSC to perform image classifications at the same rate. The case study used optical specifications for a system that has capabilities similar to the Airborne Visible/Infrared Imaging Spectrometer (AVIRIS) aboard a Twin-Otter aircraft. The results indicate that the SSC will require a processing capacity of 13 million multiply-accumulate cycles per second (MMACS) to classify hyperspectral images at a rate that exceeds the image capture capacity of the case study system. This requirement represents only 3% of the processing capacity available from state-of-the-art mobile computing platforms, including smartphones. UASs utilize most of the available computing capacity for navigational controls and communications. The SAM will require 98% of the available processing capacity to provide hyperspectral image classifications at the same rate of the SSC. Hence, the reduced complexity of the SSC will enable longer flight endurance by trading off excess capacity for lower power consumption.

The results of this research motivate the need for future studies to characterize the trade-off in sensitivity and selectivity of schemes for rapid hyperspectral image classification. In particular, the researchers will conduct field studies to establish a performance baseline using the SAM to assess classification accuracy as a function of spatial resolution. The ability to use agile UASs and the steady emergence of higher performance hyperspectral sensors will continue to enhance the sensitivity of detectors. Therefore, the authors will investigate the relationship between the achievable spatial-spectral resolutions and the sensitivity of spill detection in terms of the concentration levels detectable.

5. CONCLUSIONS

Rapid condition monitoring and performance evaluations of the vast and vulnerable transportation infrastructure has been elusive. The framework and models developed in this research will enable the next generation of transportation professionals to develop and deploy affordable and scalable solutions using evolving remote sensing technologies. This research developed an affordable framework to capture and classify hyperspectral images for transportation systems planning, analysis, and performance assessments. The rapid size and cost reduction of both unmanned aircraft systems and hyperspectral image sensors enables solution scaling by conducting multiple parallel missions to achieve broad area coverage at affordable prices. Simulations of the rapid hyperspectral image classification method of the remote sensing framework demonstrated that a resolution agile and real-time detection system is possible with small unmanned aircrafts. Such a capability will enable many new applications in transportation planning and performance evaluations.

6. REFERENCES

- AAR. 2014. *Freight Railroad Capacity and Investment*. Background Paper, Washington, D.C.: Association of American Railroads (AAR).
- Abid, M.E., T. Austin, D. Fox, and S.S. Hussain. 2014. *Drones, UAVs, and RPAs: An Analysis of a Modern Technology*. Student Project Report, Worcester, Massachusetts: Worcester Polytechnic Institute.
- Armstrong, John H. 1990. *The Railroad: What it is, What it Does. The Introduction to Railroading*. Omaha, Nebraska: Simmons-Boardman Publishing Corporation.
- Bajcsy, Peter, and Peter Groves. 2004. "Methodology for Hyperspectral Band Selection. " *Photogrammetric Engineering & Remote Sensing* (American Society Photogrammetry & Remote Sensing) 70 (7): 793-802. doi:None.
- Baldrige, A. M., S.J. Hook, C.I. Grove, and G. Rivera. 2009. "The ASTER Spectral Library Version 2.0." *Remote Sensing of Environment* (Elsevier) 113: 711-715.
- Barry, Pamela. 2001. *EO-1/Hyperion Science Data User's Guide: Level 1_B*. HYP.TO.01.077, Redondo Beach, CA: TRW Space, Defense & Information Systems, 60.
- Berger, Ivan. 2014. "Drone Control." *The Institute*, October 13.
- Bhaskaran, Sunil, and Bisun Datt. 2000. "Applications of Hyperspectral Remote Sensing in Urban Regions." *Proceedings of the 21st Asian Conference on Remote Sensing*. Taipei, Taiwan: Asian Association on Remote Sensing. 620.
- Borengasser, Marcus, William S. Hungate, and Russell Watkins. 2010. *Hyperspectral Remote Sensing: Principles and Applications*. Boca Raton, Florida: CRC Press.
- Bowen, B., K. Vlasek, and C. Webb. 2004. "An Assessment of Remote Sensing Applications in Transportation." *45th Annual Transportation Research Forum*. Fargo, ND: Transportation Research Forum. 64-96.
- Brecher, A., V. Noronha, and M. Herold. 2003. "UAV2003 - A Roadmap for Deploying Unmanned Aerial Vehicles (UAVs) in Transportation." *Volpe Center and NCRST Infrastructure Specialist Workshop (Santa Barbara, California)*. Cambridge, Massachusetts: The Volpe Center. 17.
- Bridgelall, Raj. 2014. "A participatory sensing approach to characterize ride quality." *Proceedings of SPIE Volume 9061, Sensors and Smart Structures Technologies for Civil, Mechanical, and Aerospace Systems*. Bellingham, Washington: International Society for Optics and Photonics (SPIE). doi:10.1117/12.2046854.
- Bridgelall, Raj. 2014. "Connected Vehicle Approach for Pavement Roughness Evaluation." *Journal of Infrastructure Systems* (American Society of Civil Engineers) 20 (1): 04013001 (1-6). doi:10.1061/(ASCE)IS.1943-555X.0000167.
- . 2013. "RAILCOTS -- Rolling Stock Automatic In-Situ Line-Quality, Car Operations and Tracking System." *Sensors Expo & Conference*. Chicago, IL: Questex.
- . 2014. "Remote Sensing of Oilfield Logistics with Unmanned Aircraft Systems." *Sensors Expo and Conference*. Rosemont, IL.
- Bridgelall, Raj, James Bruce Rafert, and Denver Tolliver. 2015. "Hyperspectral Imaging Utility for Transportation Systems." *SPIE Smart Structures/NDE 2015: Sensors and Smart Structures Technologies for Civil, Mechanical, and Aerospace Systems*. San Diego, California: SPIE. In Press.

- BTS. 2014. *National Transportation Statistics*. U.S. Department of Transportation, Research and Innovative Technology Administration, Washington, D.C.: Bureau of Transportation Statistics (BTS). http://www.rita.dot.gov/publications/national_transportation_statistics.
- Cambridge Systematics, Inc. 2011. *Determining Highway Maintenance Costs*. NCHRP Report 688, Washington, D.C.: Transportation Research Board (TRB).
- Cheng, Yao-Ting. 2000. *TMS320C6000 Integer Division*. Application Report SPRA707, Richardson, TX: Texas Instruments, Inc.
- Clark, R.N., G.A. Swayze, I. Leifer, K.E Livo, R. Kokaly, T. Hoefen, S. Lundeen, et al. 2010. *A Method for Quantitative Mapping of Thick Oil Spills Using Imaging Spectroscopy*. Open-File Report 2010-1167, U.S. Department of the Interior, Reston, Virginia: U.S. Geological Survey, 54.
- Clark, Roger N., K. E. Livo, and R. F. Kokaly. 1998. "Geometric Correction of AVIRIS Imagery using On-Board Navigation and Engineering Data." *Summaries of the Seventh Annual JPL Airborne Earth Science Workshop*. Pasadena, California: Jet Propulsion Laboratory (JPL), National Aeronautics and Space Administration (NASA). 57-65.
- Cloutis, E.A. 1989. "Spectral Reflectance Properties of Hydrocarbons: Remote-Sensing Implications." *Science* (American Society for the Advancement of Science) 245 (4914): 165-168.
- Cole, Bernard. 2014. "STMicro, ARM Do a Double Whammy with New Cortex-M7 Core." *Embedded.com*, September 24. Accessed April 25, 2015. www.embedded.com.
- Colomina, I., and P. Molina. 2014. "Unmanned Aerial Systems for Photogrammetry and Remote Sensing: A Review." *ISPRS Journal of Photogrammetry and Remote Sensing* (Elsevier B.V.) 92: 79-97. doi:doi:10.1016/j.isprsjprs.2014.02.013.
- Coulter, D., P. L. Hauff, and W. L. Kerby. 2007. "Airborne Hyperspectral Remote Sensing." *Proceedings of the 5th Decennial International Conference on Mineral Exploration*. Toronto, Canada: Decennial Mineral Exploration Conferences. 375-378.
- Craft, Ralph. 2004. *Crashes Involving Trucks Carrying Hazardous Materials*. FMCSA-RI-04-024, United States Department of Transportation, Washington, D.C.: Federal Motor Carrier Safety Administration (FMCSA), 8.
- Damm, A., P. Hostert, and S. Schiefer. 2005. "Investigating Urban Railway Corridors with Geometric High Resolution Satellite Data." *Urban Remote Sensing* 5.
- Dobson, Richard J., Timothy Colling, Colin Brooks, Chris Roussi, Melanie Kueber Watkins, and David Dean. 2014. "Collecting Decision Support System Data Through Remote Sensing of Unpaved Roads." *Transportation Research Record: Journal of the Transportation Research Board* (Transportation Research Board) (2433): 108-115.
- Du, Qian, and James E. Fowler. 2008. "Low-complexity Principal Component Analysis for Hyperspectral Image Compression." *International Journal of High Performance Computing Applications* (Sage Publications) 22 (4): 438-448. doi:10.1177/1094342007088380.
- Electricore, Inc. 2007. *Consolidated Research and Development for Pipeline Safety*. PHMSA Contract DTPH56-05-T-004, Valencia, California: Electricore, Inc., 47.
- FAA. 2014. *Press Release – U.S. Transportation Secretary Foxx Announces FAA Exemptions for Commercial UAS Movie and TV Production*. September 25. Accessed October 12, 2014. www.faa.gov/news/press_releases.
- Federal Aviation Administration. 2016. *Summary of Small Unmanned Aircraft Rule (Part 107)*. FAA News, Washington, D.C.: Federal Aviation Administration. http://www.faa.gov/uas/media/Part_107_Summary.pdf.

- GAO. 2014. *Oil and Gas Transportation: Department of Transportation is Taking Action to Address Rail Safety, But Additional Actions are Needed to Improve Pipeline Safety*. GAO-14-667, Washington, D.C.: Government Accountability Office (GAO).
- Gao, Hongmin, Lizhong Xu, Chenming Li, Aiye Shi, Fengchen Huang, and Zhenli Ma. 2013. "A New Feature Selection Method for Hyperspectral Image Classification Based on Simulated Annealing Genetic Algorithm and Choquet Fuzzy Integral." *Mathematical Problems in Engineering* (Hindawi Publishing Corporation).
- Gilder, George F. 2005. *The Silicon Eye*. New York, New York: WW Norton & Company.
- Goetz, Alexander F.H. 2009. "Three Decades Of Hyperspectral Remote Sensing of the Earth: A Personal View." *Remote Sensing of Environment* (Elsevier) 113: S5-S16.
- Gomez, Richard B. 2002. "Hyperspectral Imaging: A Useful Technology for Transportation Analysis." *Optical Engineering* 41 (9): 2137-2143.
- HCM. 2000. *Highway Capacity Manual (HCM), 4rd Edition*. Washington, D.C.: Transportation Research Board (TRB).
- Heiden, U., K. Segl, S. Rossner, and H. Kaufmann. 2007. "Determination of Robust Spectral Features for Identification of Urban Surface Materials in Hyperspectral Remote Sensing Data." *Remote Sensing of Environment* (Elsevier Inc.) 111 (4): 537-552.
- Herold, M., D. Roberts, V. Noronha, and O. Smadi. 2008. "Imaging Spectrometry and Asphalt Road Surveys." *Transportation Research Part C: Emerging Technologies* (Elsevier Inc.) 16 (2): 153-166. doi:10.1016/j.trc.2007.07.001.
- Herold, Martin, M. Gardner, Val Noronha, and D. Roberts. 2003. "Spectrometry and Hyperspectral Remote Sensing of Urban Road Infrastructure." Edited by Don Flournoy. *Online Journal of Space Communications* (Society for Satellite Professionals International) (3).
- Homayouni, S., and M. Roux. 2004. "Hyperspectral Image Analysis for Material Mapping Using Spectral Matching." *ISPRS Congress Proceedings*.
- Jengo, Christopher M., David Hughes, Joseph D. LaVeigne, and Ivan Curtis. 2005. "Pothole Detection and Road Condition Assessment using Hyperspectral Imagery." *Proceedings of the American Society for Photogrammetry & Remote Sensing (ASPRS) 2005 Annual Conference*. Bethesda, Maryland: American Society Photogrammetry & Remote Sensing. 7-11.
- Jensen, Austin M., Yang Quan Chen, Mac McKee, Thomas Hardy, and Steven L. Barfuss. 2009. "AggieAir - A Low-Cost Autonomous Multispectral Remote Sensing Platform: New Developments and Applications." *IEEE International Geoscience and Remote Sensing Symposium*. Hoboken, NJ: Institute of Electrical and Electronics Engineers. IV-995.
- Kiefner & Associates, Inc. 2012. *Leak Detection Study - DTPH56-11-D-000001*. Washington, D.C.: PHMSA.
- Lambrechts, Andy, Klaas Tack, and Francesco Pessolano. 2011. "Multispectral/Hyperspectral Imaging-CMOS Takes Hyperspectral Imaging Beyond the Laboratory." *Laser Focus World* (Pennwell Corporation) 47 (5): 94.
- Lambrechts, Andy, Pilar Gonzalez, Bert Geelen, Philippe Soussan, Klaas Tack, and Murali Jayapala. 2014. "A CMOS-Compatible, Integrated Approach to Hyper- and Multispectral Imaging." *Electron Devices Meeting (IEDM), 2014 IEEE International*. Piscataway, New Jersey: Institute of Electrical and Electronic Engineers (IEEE). 10.5.1 - 10.5.4.
- Landgrebe, David. 2002. "Hyperspectral Image Data Analysis." *Signal Processing Magazine* (Institute of Electrical and Electronic Engineers) 19 (1): 17-28. doi:10.1109/79.974718.

- Mah, Steven, Jennifer Aitken, Karen Schuckman, and Charles O'Hara. 2002. "CASI/Lidar Sensor Fusion for Wetland Classification." *15th William T. Pecora Memorial Remote Sensing Symposium/Land Satellite Information IV Conference and Exhibition*. Denver, Colorado: International Society for Photogrammetry and Remote Sensing.
- Mather, Paul, and Brandt Tso. 2003. *Classification Methods for Remotely Sensed Data*. Boca Raton, Florida: CRC Press (Taylor & Francis).
- McIntee, Erin Maureen. 2008. *Forensic Analysis of Automobile Paints by Atomic and Molecular Spectroscopic Methods and Statistical Data Analyses*. Doctoral Dissertation, Orlando, Florida: University of Central Florida, 102.
- Meer, Freek D. Van der, Harald van der Werff, Frank JA van Ruitenbeek, Chris A. Hecker, Wim H. Bakker, Marleen F. Noomen, Mark van der Meijde, John M. Carranza, J. Smeth, and Tsehaie Woldai. 2012. "Multi- and hyperspectral geologic remote sensing: A review." *International Journal of Applied Earth Observation and Geoinformation* (Elsevier) 14 (1): 112-128.
- Mei, Alessandro, Rosamaria Salvatori, Nicola Fiore, Alessia Allegrini, and Antonio D'Andrea. 2014. "Integration of Field and Laboratory Spectral Data with Multi-Resolution Remote Sensed Imagery for Asphalt Surface Differentiation." *Remote Sensing* (Multidisciplinary Digital Publishing Institute) 6 (4): 2765-2781.
- Mohammadi, M., M. Hahn, and J. Engels. 2011. "Road Classification and Condition Investigation Using Hyperspectral Imagery." *Applied Geoinformatics for Society and Environment (AGSE 2011)*. Nairobi, Kenya: Jomo Kenyatta University of Agriculture and Technology.
- Muller, Jean-Michel. 2006. *Elementary Functions: Algorithms and Implementation*. Berlin, Heidelberg: Springer Science & Business Media.
- Muslimov, É. R. 2014. "A Monolithic Spectrograph with a Transmissive Holographic Diffraction Grating." Edited by A.S. Tibilov. *Journal of Optical Technology* (Vavilov State Optical Institute) 81 (3): 154-158.
- NAPA; EAPA. 2009. *The Asphalt Paving Industry: A Global Perspective*. Global Series 101, Brussels: National Asphalt Pavement Association (NAPA) and the European Asphalt Pavement Association (EAPA).
- NIST. June. *Forensic Database Trace Evidence Table*. National Institute of Standards and Technology (NIST). 4 2013. Accessed May 27, 2015. <http://www.nist.gov/oles/forensics/forensic-database-trace-evidence-table.cfm>.
- Palenik, C.S., S. Palenik, E. Groves, and J. rb. 2014. *Raman Spectroscopy of Automotive and Architectural Paints: In situ Pigment Identification and Evidentiary Significance*. Study Sponsored by the U.S. Department of Justice, Washington, D.C.: Microtrace, LLC.
- Pearlman, J., S. Carman, C. Segal, P. Jarecke, P. Barry, and W. Browne. 2001. *Overview of the Hyperion Imaging Spectrometer for the NASA EO-1 Mission*. Washington, D.C.: National Air and Space Administration (NASA).
- Penn, B.S. 2002. "Using Hyperspectral Imagery to Map Roads and Determine Surface Material Types." *15th William T. Pecora Memorial Remote Sensing Symposium/Land Satellite Information IV Conference and Exhibition*. Denver, Colorado: International Society for Photogrammetry and Remote Sensing.
- Prats-M., J.M., A. De Juan, and A. Ferrer. 2011. "Multivariate Image Analysis: A Review with Applications." *Chemometrics and Intelligent Laboratory Systems* (Elsevier Inc.) 107 (1): 1-23.

- Proto, M., M.Bsi, R. Bernini, L. Bigagli, M. Bost, F. Bourquin, and L. Cottineau. 2010. "Transport Infrastructure Surveillance and Monitoring by Electromagnetic Sensing: The ISTIMES Project." *Sensors* (European Commission) 10 (12).
- Puri, A. 2005. *A Survey of Unmanned Aerial Vehicles (UAV) for Traffic Surveillance*. Project Report, Department of Computer Science and Engineering, Tampa, Florida: University of South Florida, 29.
- Rafert, B.J. 2014. "Before Hyperspectral Ruled the World." *Hyperspectral Imaging and Applications Conference*. Glasgow, U.K.: University of Strathclyde.
- Rani, S. 2014. "Monitoring Land Use/Land Cover Response to Urban Growth of the city of Jalandhar using Remote Sensing Data." *International Journal of Advanced Research* 2 (6): 1122-1129.
- Resende, M.R., L.L.Bariani Bernucci, and José Alberto Quintanilha. 2014. "Monitoring the Condition of Roads Pavement Surfaces: Proposal of Methodology Using Hyperspectral Images." *Journal of Transport Literature* (Brazilian Transport Planning Society) 8 (2): 201-220.
- Richards, J.A. 1999. *Remote Sensing Digital Image Analysis*. Berlin: Springer-Verlag.
- Roess, R.P., E. S. Prassas, and W.R. McShane. 2011. *Traffic Engineering*. 4th. Upper Saddle River, New Jersey: Pearson Higher Education, Inc.
- Salem, F. and M. Kafatos. 2001. "Hyperspectral Image Analysis for Oil Spill Mitigation." *The 22nd Asian Conference on Remote Sensing*. Singapore: Center for Remote Imaging, Sensing, and Processing (CRISP), National University of Singapore. 9.
- Smejkalová, E. and P. Bujok. 2012. "Remote Sensing Methods In The Identification of Oil Contaminations." *GeoScience Engineering* 58 (1): 24-33.
- Sohn, Y, and N.S. Rebello. 2002. "Supervised and Unsupervised Spectral Angle Classifiers." *Photogrammetric Engineering & Remote Sensing* (American Society Photogrammetry & Remote Sensing) 68 (12): 1271-1280.
- Sugumaran, R., J. Gerjevic, and M. Voss. 2007. "Transportation Infrastructure Extraction Using Hyperspectral Remote Sensing." *Remote Sensing of Impervious Surfaces* 163-178.
- Suzuki, E. M. and M. Carrabba. 2001. "In Situ Identification and Analysis of Automotive Paint Pigments Using Line Segment Excitation Raman Spectroscopy: I. Inorganic Topcoat Pigments." *Journal of Forensic Sciences* 46 (5): 1053-1069.
- Tarabalka, Y., J.A. Benediktsson, and J. Chanussot. 2009. "Spectral–Spatial Classification of Hyperspectral Imagery Based on Partitional Clustering Techniques." *IEEE Transactions on Geoscience and Remote Sensing* 47 (8): 2973-2987. doi:10.1109/TGRS.2009.2016214.
- Thomas, G. B. and R. L. Finney. 1995. *Calculus and Analytic Geometry*. 9th. Boston: Addison Wesley.
- TRB. 2003. *Remote Sensing for Transportation: Products and Results – Foundations for the Future*. Report of a Conference, The National Academies, Washington, D.C.: Transportation Research Board (TRB), 98.
- USDOT. 2011. *The State of the National Pipeline Infrastructure*. Washington, D.C.: United States Department of Transportation.
- . 2015. "DOT Agencies Take Coordinated Actions to Increase the Safe Transportation of Energy Products." *USDOT Bulletins*, April 17.
- Van der Werff, Harald, M. Van der Meijde, F. Jansma, F. Van der Meer, and G. Jan Groothuis. 2008. "A Spatial-Spectral Approach for Visualization of Vegetation Stress Resulting from Pipeline Leakage." *Sensors* (Multidisciplinary Digital Publishing Institute) 8 (6): 3733-3743.

- Warren, S., T. Puestow, M. Richard, and B. Jefferies. 2014. *Oil Spill Detection and Modeling in the Hudson and Davis Straits*. R-13-087-1096, St. John's, Newfoundland: LookNorth Center of Excellence for Commercialization and Research, 174.
- Yerasi, A., W. Emery. 2014. "Sensing Highway Surface Conditions with High-Resolution Satellite Imagery." *TRB Committee ABJ50 on Information Systems and Technology*. Washington, D.C.: University of Colorado at Boulder and DigitalGlobe. P14-6196.
- Zhang, C. 2013. *Monitoring the Condition of Unpaved Roads with Remote Sensing and Other Technology*. Research in Progress, Transportation Research Board (TRB), Brookings, SD: South Dakota State University.
- Zietsman, J., T. Ramani, J. Potter, V. Reeder, and J. DeFlorio. 2011. *A Guidebook for Sustainability Performance Measurement for Transportation Agencies*. NCHRP Report 708, Washington, D.C.: Transportation Research Board, 203.